Journal for ImmunoTherapy of Cancer

Heterologous prime-boost vaccination targeting MAGE-type antigens promotes tumor T-cell infiltration and improves checkpoint blockade therapy

James McAuliffe,[1] Hok Fung Chan,[1] Laurine Noblecourt,[1] Ramiro Andrei Ramirez-Valdez,[1] Vinnycius Pereira-Almeida,[1,2] Yaxuan Zhou,[1,3] Emily Pollock,[4] Federica Cappuccini,[4] Irina Redchenko,[4] Adrian VS Hill,[4] Carol Sze Ki Leung ,[1] Benoit J Van den Eynde [1,5]

To cite: McAuliffe J, Chan HF, Noblecourt L, *et al*. Heterologous prime-boost vaccination targeting MAGE-type antigens promotes tumor T-cell infiltration and improves checkpoint blockade therapy. *Journal for ImmunoTherapy of Cancer* 2021;**9**:e003218. doi:10.1136/jitc-2021-003218

► Additional supplemental material is published online only. To view, please visit the journal online (http://dx.doi.org/10.1136/jitc-2021-003218).

CSKL and BJVdE contributed equally.

Accepted 26 July 2021

For numbered affiliations see end of article.

Correspondence to
Dr Carol Sze Ki Leung; carol.leung@ludwig.ox.ac.uk

ABSTRACT

Background The clinical benefit of immune checkpoint blockade (ICB) therapy is often limited by the lack of pre-existing CD8$^+$ T cells infiltrating the tumor. In principle, CD8$^+$ T-cell infiltration could be promoted by therapeutic vaccination. However, this remains challenging given the paucity of vaccine platforms able to induce the strong cytotoxic CD8$^+$ T-cell response required to reject tumors. A therapeutic cancer vaccine that induces a robust cytotoxic CD8$^+$ T-cell response against shared tumor antigens and can be combined with ICB could improve the outcome of cancer immunotherapy.

Methods Here, we developed a heterologous prime-boost vaccine based on a chimpanzee adenovirus (ChAdOx1) and a modified vaccinia Ankara (MVA) encoding MAGE-type antigens, which are tumor-specific shared antigens expressed in different tumor types. The mouse MAGE-type antigen P1A was used as a surrogate to study the efficacy of the vaccine in combination with ICB in murine tumor models expressing the P1A antigen. To characterize the vaccine-induced immune response, we performed flow cytometry and transcriptomic analyses.

Results The ChAdOx1/MVA vaccine displayed strong immunogenicity with potent induction of CD8$^+$ T cells. When combined with anti-Programmed Cell Death Protein 1 (PD-1), the vaccine induced superior tumor clearance and survival in murine tumor models expressing P1A compared with anti-PD-1 alone. Remarkably, ChAdOx1/MVA P1A vaccination promoted CD8$^+$ T-cell infiltration in the tumors, and drove inflammation in the tumor microenvironment, turning 'cold' tumors into 'hot' tumors. Single-cell transcriptomic analysis of the P1A-specific CD8$^+$ T cells revealed an expanded population of stem-like T cells in the spleen after the combination treatment as compared with vaccine alone, and a reduced PD-1 expression in the tumor CD8$^+$ T cells.

Conclusions These findings highlight the synergistic potency of ChAdOx1/MVA MAGE vaccines combined with anti-PD-1 for cancer therapy, and establish the foundation for clinical translation of this approach. A clinical trial of ChadOx1/MVA MAGE-A3/NY-ESO-1 combined with anti-PD-1 will commence shortly.

INTRODUCTION

Recent developments in the field of immunotherapy have brought about unprecedented improvements in patient outcomes for previously difficult to treat advanced cancers. This is best exemplified by immune checkpoint blockade (ICB)—therapies targeting ligand-receptor interactions that negatively regulate effector T-cell function, or so-called immune checkpoints.[1 2] Inhibiting these immune checkpoint pathways with monoclonal antibodies (mAbs) can enhance the priming of anti-tumor T cells and restore their effector activity.[3] Immune checkpoint inhibitors, particularly those targeting PD-1, Programmed Cell Death Ligand 1 (PD-L1), or Cytotoxic T Lymphocyte-associated Antigen 4 (CTLA-4) induce durable tumor regressions and greatly enhance survival in cancer patients.[4–6] However, despite these successes, in most cancer types, the majority of patients fail to respond and do not experience clinical benefit. This is partly due to a lack of pre-existing antitumor CD8$^+$ cytotoxic T lymphocytes (CTLs).[7] Therapeutic cancer vaccines that can generate CTLs against tumor-specific antigens could therefore improve response rates to ICB. Indeed, the concept of combining ICB with therapeutic cancer vaccination has been tested in the clinic, with vaccination targeting the tumor-causing human papillomavirus.[8]

Melanoma antigen gene (MAGE)-type antigens are tumor-specific antigens that have long been the targets of cancer vaccines due to their unique properties.[9] They are non-mutated antigens encoded by cancer-germline genes, whose expression in normal tissues is mostly restricted to male germline cells that are incapable of presenting antigens

to the immune system due to the lack of Human Leukocyte Antigen (HLA) molecules.[9] Being non-mutated, these antigens are shared by many independent tumors and found in a high proportion of human tumors, as opposed to mutated neoantigens. Peptides derived from MAGE-type proteins are presented by HLA molecules to tumor-specific T lymphocytes, and antitumor $CD8^+$ T cells from many different patients with cancer were found to recognize MAGE-type antigens,[10–12] indicating that these antigens are highly immunogenic. Previous attempts to develop MAGE-targeting cancer vaccines however have proven unsuccessful, with candidates failing to demonstrate significant efficacy in large-scale clinical trials.[13 14] These studies used a classical vaccine platform with recombinant MAGE-A3 protein and adjuvant formulations, which preferentially induces antibody and $CD4^+$ T-cell responses rather than the strong $CD8^+$ CTL responses necessary for significant antitumor effect.[15 16]

In contrast to traditional vaccine platforms, recombinant viral vector vaccines have recently been shown to induce potent $CD8^+$ T-cell responses in humans.[17] In particular, heterologous prime-boost vaccines using chimpanzee adenovirus ChAdOx1 and modified vaccinia Ankara (MVA) were shown to generate some of the highest magnitude $CD8^+$ T-cell responses against antigens in the settings of infectious diseases and prostate cancer.[17–19] Head-to-head comparisons of multiple platforms have shown the advantage of adenoviral/MVA prime-boost vaccination schemes for inducing $CD8^+$ T-cell responses against a tumor-associated viral antigen.[20] Though these studies can demonstrate adenoviral/MVA prime-boost vaccination is superior in stimulating peripheral antitumor CTL responses, its effect on the tumor microenvironment (TME) is not well explored. The presence of $CD8^+$ T cells and associated inflammation in tumors is linked to improved prognoses and is vital for a positive clinical response to ICB.[7] T-cell inflamed tumor gene expression signatures are better predictors of response than all other variables.[21 22] An effective therapeutic cancer vaccine should therefore be able to promote $CD8^+$ T-cell infiltration into the tumor and induce inflammation in the TME, turning a 'cold' non-inflamed tumor 'hot'. Thus, cancer vaccines have the potential to work synergistically with ICB to improve their efficacy.

Here, we generated recombinant ChAdOx1 and MVA vectors expressing the prototypical MAGE-type antigens MAGE-A3, NY-ESO-1 or their murine counterpart P1A,[23] which shares strong similarities with human MAGE-type antigens including the pattern of expression.[24] The immunogenicity and anti-tumor efficacy of the ChAdOx1/MVA P1A vaccine with and without checkpoint inhibitors was evaluated in mouse tumor models. We show that the ChAdOx1/MVA P1A vaccine boosts the levels of P1A-specific $CD8^+$ tumor-infiltrating lymphocytes (TILs) in an otherwise poorly infiltrated tumor, and enhances response to anti-PD-1 blockade, resulting in better tumor control and improved survival. Finally, we assessed the immunogenicity of the ChAdOx1/MVA MAGE-A3-NY-ESO-1 vaccines to support an imminent clinical trial study.

MATERIALS AND METHODS

Mice

Six to eight-week-old female CD1, C57BL/6 and DBA/2 mice used in this study were purchased from Envigo, UK.

Viral vectors

The coding sequence of P1A (NCBI RefSeq NP_035765.1), MAGE-A3 (NCBI RefSeq NM_005362.3) and NY-ESO-1 (GenBank: U87459.1) were purchased as strings DNA fragments from GeneArt (Thermo Fisher Scientific, Paisley, UK). Further details on vector construction are described in the online supplemental materials.

Vaccinations and immune checkpoint inhibitor treatments

Vaccinations were performed at a dose of either 10^8 or 10^7 infectious units of ChAdOx1 virus and 10^7 or 10^6 plaque forming units of MVA virus, given via intramuscular (i.m.) injection in 50 µL total volume. Anti-PD-1 (BioXcell, clone RMP114), anti-CTLA-4 (BioXcell, clone 9H10) or the relevant isotype control (BioXcell, clone 2A3) were administered via intraperitoneal injection at a dose of 100 µg per mouse, given 3 times at a 3-day interval. For therapeutic efficacy studies, tumor-bearing mice were randomized according to tumor size before treatment.

Cell lines, tumor transplantation and measurements

P815 and 15V4T3 cell lines are of DBA/2 origin and express P1A.[25] B16F10 and MC38 cell lines were obtained from ATCC. Cell lines were regularly mycoplasma tested to confirm the absence of infection. To initiate tumor growth, 1×10^6 (15V4T3, P815) or 1×10^5 (B16F10, MC38) tumor cell suspension was implanted subcutaneously (s.c.) in the right flank of the mice. Tumor growth was measured 2–3 times per week and mice were sacrificed when tumor size reached 10 mm or 12 mm in any direction. Tumor volume (V) was calculated according to the formula: $V = ((\text{length (mm)} \times \text{width}^2\ \text{(mm)}) \times 0.52)$. For mean tumor volume calculations, the final end-point value recorded when a mouse was sacrificed was carried forward to enable the calculation of a group mean at later time points.

Surface staining, intracellular cytokine staining and flow cytometry

Peripheral blood mononuclear cells (PBMCs) and bulk splenocytes were harvested as described previously.[26] Tumor masses were surgically excised and weighed. Tumor single cell suspension was obtained by dissociation of tissues using a gentleMACS Dissociator (Miltenyi Biotec) according to the manufacturer's instruction. For surface staining, cells were incubated for 10 min at 4°C with 5 µg/mL anti-CD16/CD32 (clone 2.4G2, BD Biosciences) to block Fc receptors, washed, and then stained for 30 min at 4°C with PE-conjugated

H-2L^d/P1A$_{35-43}$- LPYLGWLVF multimer (manufactured and provided by Ludwig Institute for Cancer Research, Brussels, Belgium). Cells were then washed and stained for 20 min at 4°C with viability dye (LIVE/DEAD Aqua, Invitrogen) and fluorescently conjugated mAbs against surface molecules according to different staining panels; anti-CD3-APC (clone 17A2), anti-CD8-FITC (clone 53–6.7), anti-CD4-AlexaFluor-700 (clone GK1.5), anti-PD-1-PE-Cy7 (clone 29F.1A12), anti-TIM-3-BV421 (clone RMT3-23), anti-LAG-3-BV650 (clone C9B7W), anti-CD11b-FITC (clone M1/70), anti-CD11c-BV650 (clone N418), anti-F4/80-BV421 (clone BM8), anti-Ly6C-APC (clone HK1.4), anti-Ly6G-PE-Cy7 (clone 1A8). For intracellular cytokine staining (ICS), cells were stimulated with 4 µg/mL of MAGE-A3, NY-ESO-1 or P1A 15-mer peptide mix (PepSets Peptide library, Mimotopes) in the presence of DNaseI (20 µg/mL, Roche) and costimulatory anti-CD28 (2 µg/mL, Tonbo Biosciences) at 37°C for 5 hours, adding brefeldin A (10 µg/mL, BioLegend) for the last 4 hours to allow accumulation of intracellular cytokines. Cells were then surface stained, fixed and permeabilized (BD Cytofix/Cytoperm), then stained intracellularly for cytokine production with anti-IFN-γ-APC (clone XMG1.2), anti-IL-2-PE (clone JES6-5H4), and anti-TNF-α-BV650 (clone MP6-XT22), and then acquired on a Fortessa flow cytometer (BD Biosciences). All mAbs were purchased from BioLegend. Data were analyzed with FlowJo software v10 (Tree Star, Ashland, Oregon). Analysis of multifunctional CD8$^+$ T-cell responses was performed via a Boolean analysis of IFN-γ$^+$, TNF-α$^+$, IL-2$^+$ events in the CD8$^+$ gate using FlowJo. Pestle (NIH, Bethesda) and SPICE (Vaccine Research Centre, NIH, Bethesda) software were used to generate graphical representations of proportions of T cells expressing 1, 2 or all 3 cytokines.

RNA sequencing

For bulk RNA sequencing, sample cDNA libraries were prepared following poly-A selection to enrich for mRNA and then sequenced as 150 bp paired-end reads on a NovaSeq 6000 (Illumina). For scRNA-seq, tumors and spleens were processed into single cell suspension. Biological replicates (n=10) for each experimental condition were pooled together at the tissue processing stage. Around 5000 live CD3$^+$CD8$^+$P1A$_{35-43}$-LPYLGWLVF$^+$ cells from each condition were sorted by fluorescence activated cell sorting using a BD FACSAria III (BD Biosciences). Sorted cells from each experimental condition were loaded into a Chromium single-cell sorting system (10× Genomics). Single-cell RNA libraries were prepared using 10× Genomics Chromium platform and reagents according to the manufacturer's instructions by the Oxford Genomics Centre, University of Oxford. Details of sequencing data analysis are described in the online supplemental materials.

Statistical analysis

Statistical analyses were carried out using Prism v8.0 (GraphPad). For immunogenicity study data, to determine significance comparing between multiple groups a Kruskal-Wallis test with a Dunn's post hoc analysis was performed. For comparisons between only two groups a Mann-Whitney U-test was performed. To determine significance between responses at different time-points within the same group a Wilcoxon matched-pairs signed rank tested was performed. For gene expression studies, ordinary one-way analysis of variance (ANOVA) was performed followed by Tukey's post hoc to determine significance between individual groups. Statistically significant differences in tumor growth between different groups was determined by two-way ANOVA followed by Tukey's post hoc test. Survival curves were created using the Kaplan-Meier method and statistical significance between different groups was determined using the log-rank (Mantel-Cox) test. All p values<0.05 were considered statistically significant.

RESULTS

ChAdOx1/MVA P1A prime-boost vaccination induces robust P1A-specific CD8$^+$ T-cell responses

We first evaluated the immunogenicity of the ChAdOx1/MVA vectors encoding the murine MAGE-type antigen P1A, and the effect of the molecular adjuvants, namely the MHC-class II-associated invariant chain transmembrane domain (Ii-TMD) and the tissue plasminogen activator (tPA) signal sequence.[27 28] DBA/2 mice were given a ChAdOx1-P1A (±Ii) prime vaccination and then received an MVA-P1A boost vaccination 4 weeks later (figure 1A). PBMCs from vaccinated mice were stimulated with overlapping P1A peptides and the fraction of cytokine-producing P1A-specific CD8$^+$ T cells assessed by flow cytometry (figure 1B). Following prime vaccination with either ChAdOx1-P1A or ChAdOx1-Ii-P1A, significantly higher frequencies of IFN-γ-producing CD8$^+$ T cells were detected compared with the PBS control group (figure 1C). Notably, fusion of the Ii-TMD sequence to P1A increased the frequencies of P1A-specific CD8$^+$ T cells induced by ChAdOx1 vaccination. Furthermore, the MVA-P1A boost greatly increased the magnitude of the P1A-specific CD8$^+$ T-cell response (figure 1C). No P1A-specific CD4$^+$ T-cell response was observed, in line with the fact that no CD4 epitope has been described for P1A (online supplemental figure S1A). Frequencies of H-2L^d P1A$_{35-43}$-LPYLGWLVF$^+$ CD8$^+$ T cells post MVA vaccination were similar to frequencies of IFN-γ$^+$ CD8$^+$ T cells detected by ICS, further confirming induction of a strong P1A-specific CD8$^+$ T-cell response (figure 1D). While more than 50% of the vaccine-induced CD8$^+$ T cells were polyfunctional, producing at least two cytokines among IL-2, TNF-α and IFN-γ, we did not detect any significant differences between different groups (figure 1E). The inclusion of tPA to P1A in the MVA vector did not significantly alter

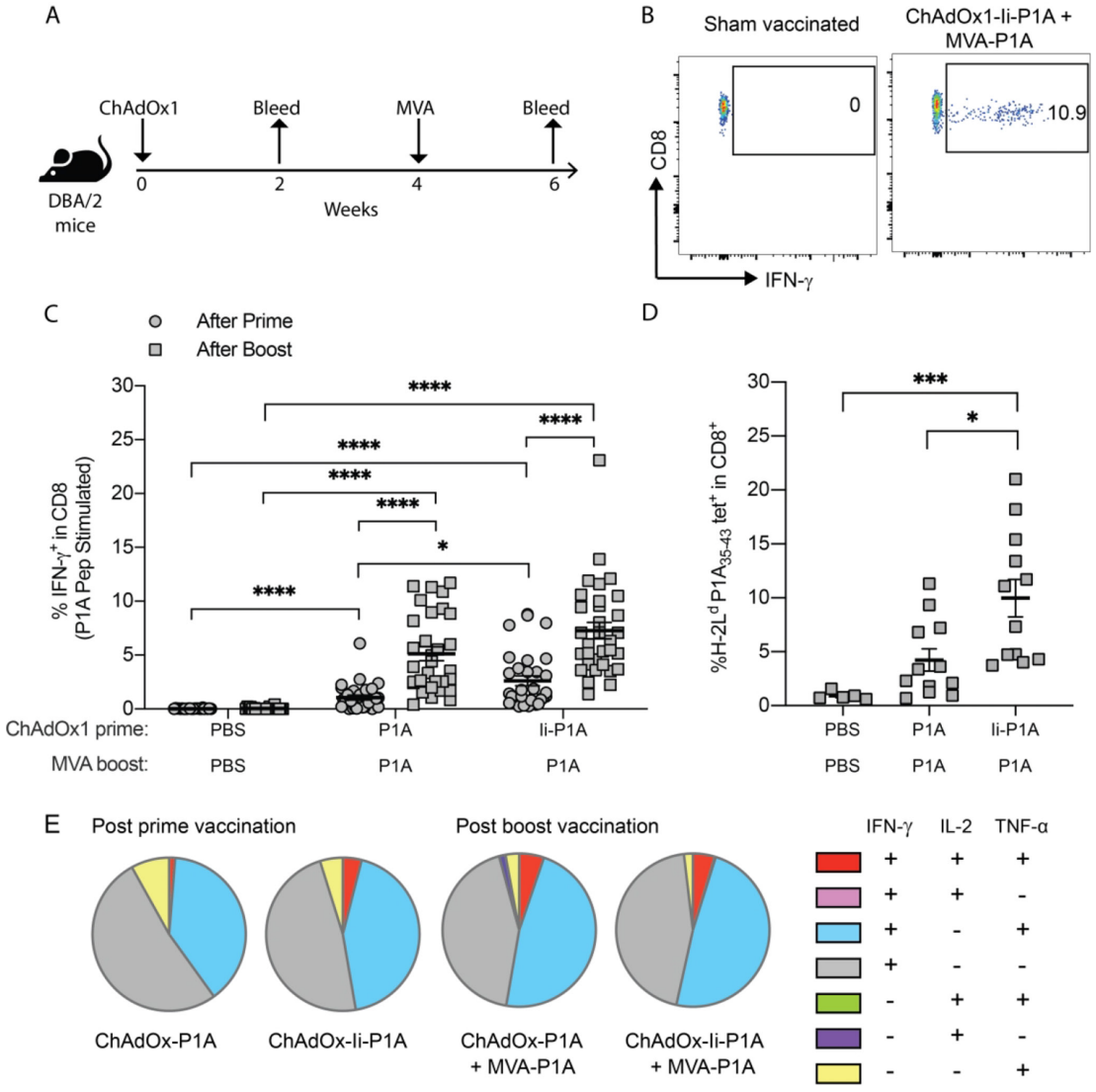

Figure 1 ChAdOx1/MVA P1A vaccination induces robust P1A-specific CD8$^+$ T-cell responses. DBA/2 mice received a prime vaccination via intramuscular (i.m.) injection with 10^8 IU of ChAdOx1-P1A ± li or a sham vaccination with PBS then 4 weeks later received a boost vaccination with 10^7 PFU of MVA-P1A. Mice were bled 10-20 days after vaccination with ChAdOx1 and 9-14 days after vaccination with MVA. (A) Experimental scheme. (B) PBMCs were stimulated *ex vivo* with 4 µg/ml of P1A peptide pools and the percentage of cytokine-producing P1A-specific CD8$^+$ T cells in the blood after each vaccination was then determined by intracellular cytokine staining (ICS) and flow cytometry. The representative dot plots show gating of IFN-γ$^+$ CD8$^+$ T cells. (C, D) Percentages of IFN- γ$^+$ cells among CD8$^+$ T cells after prime (closed circles) and boost (closed squares) are shown in (C) and percentages of $P1A_{35-43}$ tetramer$^+$ CD8$^+$ T cells after boost are shown in (D). Data are shown as mean ± SEM, each symbol represents an individual mouse with 5-10 mice per group, pooled from 2-4 independent experiments. Statistically significant differences between groups were determined by a Kruskal-Wallis test with Dunn's multiple comparisons test. *, p ≤ 0.05, ***, p ≤ 0.001 ****, p ≤ 0.0001. (E) Cytokine production profile of P1A-specific CD8$^+$ T cells is shown. A Boolean analysis was performed in FlowJo software to calculate the percentage of CD8$^+$ T cells producing only one, a combination of two, or all three of IFN-γ, IL-2 and TNF-α. Pie charts show the mean relative proportion of each cytokine producing subset out of the total antigen-specific CD8$^+$ T cells.

the frequencies of vaccine-induced P1A-specific CD8$^+$ T cells (online supplemental figure S1B).

ChAdOx1/MVA P1A vaccination exhibits good therapeutic efficacy against early established 15V4T3 tumors

The high magnitude P1A-specific CD8$^+$ T-cell responses induced by ChAdOx1/MVA P1A vaccination translated into tumor protection when vaccinated mice were challenged with tumor cells from either P815 or 15V4T3, two P1A-expressing mastocytoma cell lines[25 29] (online supplemental figure S2A-E). Then, we further tested the vaccine therapeutic efficacy against 15V4T3 tumors, which showed lower rates of spontaneous tumor resolution than P815 (online supplemental figure S2F). Three different ChAdOx1/MVA P1A vaccination doses and schedules, aimed at shortening vaccination time, were tested against early established 15V4T3

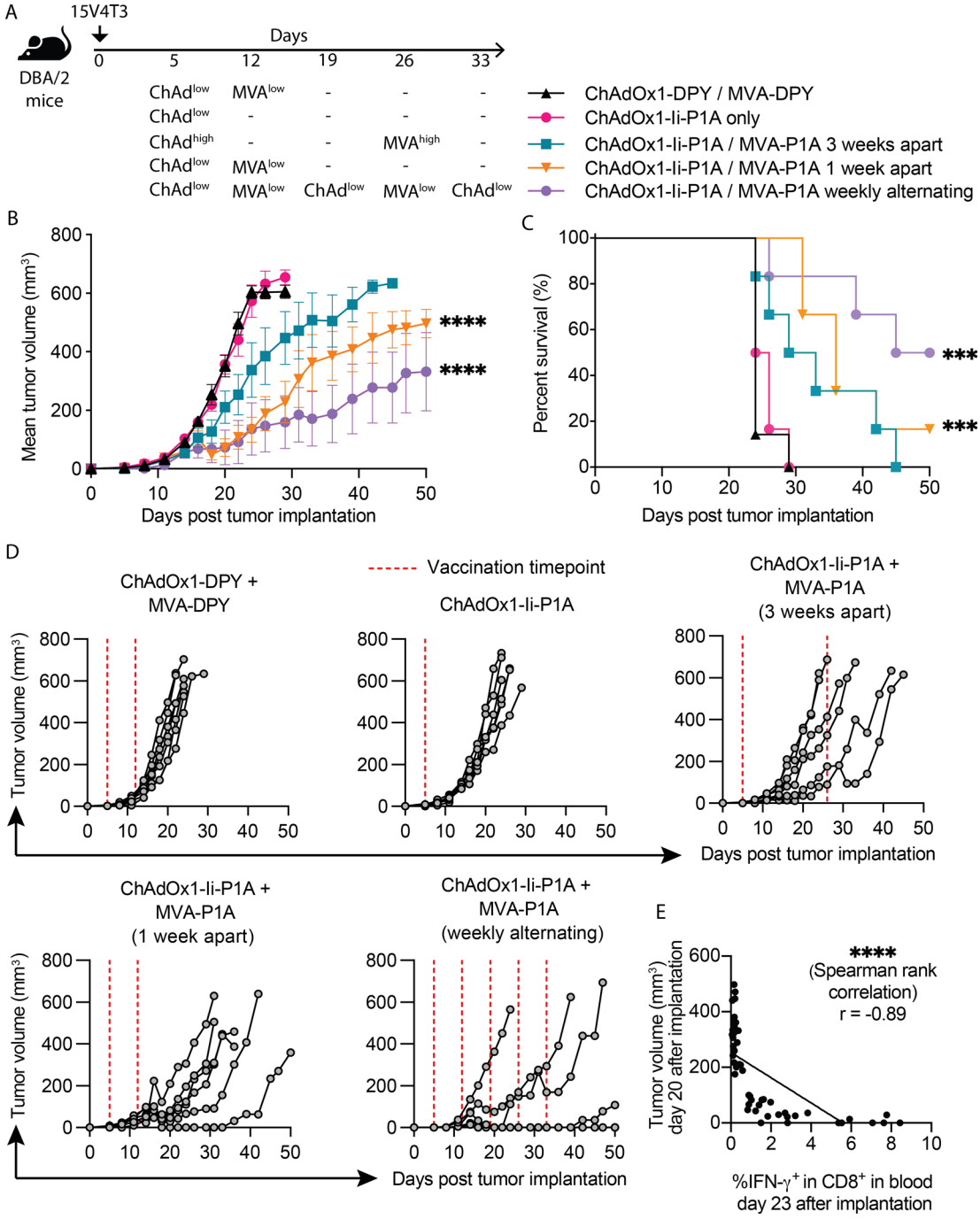

Figure 2 ChAdOx1/MVA P1A vaccination exhibits good therapeutic efficacy against early established 15V4T3 tumors. (A) DBA/2 mice were implanted with $1x10^6$ 15V4T3 cells via subcutaneous (s.c.) injection. Five days after tumor implantation, mice were vaccinated with ChAdOx1-li-P1A and MVA-P1A according to the schedules shown and indicated doses of virus: $ChAd^{high}$ - 10^8 IU, $ChAd^{low}$ - 10^7 IU, MVA^{high} - 10^7 PFU and MVA^{low} - 10^6 PFU. Tumor growth was followed for 50 days and mice culled when tumors reached 12 mm in any direction. (B-D) Mean tumor growth (B), survival (C) and individual tumor growth (D) for each group are shown. (E) Tumor size on day 20 post implantation was correlated with the frequency of blood IFN-γ^+ $CD8^+$ T cells detected by *ex vivo* P1A peptide stimulation and ICS on day 23. Tumor growth data are presented as mean tumor volume (mm^3) ± SEM. Each group contained 6-7 mice, with data representative of 2 independent experiments. Statistically significant differences between groups were determined by a two-way ANOVA with Tukey's post hoc test for tumor volume data and a log-rank test for survival data. Statistical differences are shown only between vaccinated groups and ChAdOx/MVA control group. Significance of correlation was determined through a Spearman rank test. ***, $p \leq 0.001$ ****, $p \leq 0.0001$.

tumors (5 days after implantation), with a control group receiving ChAdOx1/MVA expressing irrelevant protein DPY (figure 2A). Compared with the control group, mice receiving ChAdOx1/MVA P1A vaccinations showed improved control of 15V4T3 tumor growth (figure 2B,D). Mice in the control group had

mostly succumbed to tumor burden within 24 days post tumor implantation. Conversely mice receiving low-dose ChAdOx1/MVA P1A vaccinations, either given 1 week apart or weekly alternating vaccinations, had significantly improved tumor control and longer survival (figure 2B–D). This was most apparent in the groups receiving weekly alternating vaccinations. This result is in line with a previous study showing that low dose weekly alternating ChAdOx1/MVA vaccinations provided superior control of tumor growth in prostate cancer models.[30] A single log-fold reduced dose of ChAdOx1-Ii-P1A did not demonstrate a therapeutic effect, suggesting the MVA boost to be critical for vaccine therapeutic efficacy. P1A-specific T-cell responses in the blood of tumor-bearing mice were assessed as previously by P1A peptide-stimulation and ICS of PBMCs. Interestingly, a strong negative correlation (Spearman rank, r=−0.89) was observed between tumor burden and frequencies of peripheral IFN-γ-producing CD8$^+$ T cells, suggesting that the vaccine-induced response was likely responsible for tumor control (figure 2E).

ChAdOx1/MVA P1A vaccination combined with ICB enhances tumor control

Though vaccination alone was able to control early established tumors, the majority of cancers are diagnosed at a late stage. Also, we observed PD-L1 to be constitutively expressed on the surface of 15V4T3 cells, and its expression further upregulated by IFN-γ stimulation (online supplemental figure S3A–D). Therefore, we tested the combination of vaccination with ICB against more established 15V4T3 tumors (figure 3A). Initiating vaccination at a later time-point against more established tumors (day 8 compared with day 5 in previous therapeutic experiments, figure 2) greatly reduced the therapeutic effect of ChAdOx1-Ii-P1A/MVA-P1A vaccination alone (figure 3B–D). Compared with the PBS control group, there was no significant control of tumor growth (figure 3B) and only a slight improvement in survival was observed (figure 3C). Interestingly, ICB monotherapy with either anti-PD-1 or anti-CTLA-4 alone was similarly ineffective at controlling tumor growth. Anti-PD-1 alone only delayed tumor growth (figure 3B) and increased survival by a small amount (figure 3C) compared with the PBS control. However, the combination of ChAdOx1-Ii-P1A/MVA-P1A vaccination with either anti-PD-1 or anti-CTLA-4 strongly improved tumor control over any modality given alone. Tumor growth was significantly reduced in the ChAdOx1-Ii-P1A/MVA-P1A+anti-PD-1 combination group compared with both ChAdOx1-Ii-P1A/MVA-P1A only and anti-PD-1 only groups (figure 3B), and survival was significantly improved (figure 3C). Indeed, half of the mice in the ChAdOx1-Ii-P1A/MVA-P1A+anti-PD-1 group were able to completely resolve their tumors and were still alive after 50 days (figure 3D; n=3/6). Though the combination of vaccination with anti-CTLA-4 resulted in better control of tumor growth over the respective single treatment groups, survival was not significantly increased. Further still, the combination of ChAdOx1-Ii-P1A/MVA-P1A vaccination with anti-PD-1 was more efficacious than with anti-CTLA-4; over the course of 50 days the mean tumor growth in the ChAdOx1-Ii-P1A/MVA-P1A+anti-PD-1 group was significantly less than the ChAdOx1-Ii-P1A/MVA-P1A+anti-CTLA-4 group (figure 3B). These results suggested that there was particular synergy in the combination of ChAdOx1/MVA P1A vaccination with anti-PD-1 blockade for generating a potent antitumor effect.

ChAdOx1/MVA P1A vaccination promotes CD8$^+$ T-cell infiltration and drives inflammation in the TME

We then sought to determine the effect of ChAdOx1/MVA P1A vaccination ±anti-PD-1 treatment on T-cell infiltration and inflammation in the 15V4T3 TME. First, the T-cell infiltration of 15V4T3 tumors was compared with well-defined tumor models—MC38, a 'hot' relatively T-cell inflamed and ICB responsive tumor and B16F10, a 'cold' poorly immunogenic and ICB unresponsive tumor.[31] 15V4T3 tumors were poorly infiltrated by CD8$^+$ T cells, containing on average significantly fewer TILs than MC38 tumors, and slightly fewer than even B16F10 tumors (online supplemental figure S3E,F). This extreme paucity of CD8$^+$ TILs in 15V4T3 suggests it is more akin to an immune 'cold' tumor, and this could likely underlie the low effect of anti-PD-1 treatment given as monotherapy. Next, 15V4T3 tumors were harvested from mice following vaccine ±anti-PD-1 treatment at 20 days after implantation, and the immune composition was profiled by flow cytometry (figure 4A). Tumors from mice receiving either vaccine alone or vaccine +anti-PD-1 contained significantly higher percentages and total numbers of CD8$^+$ TILs compared with the PBS control and anti-PD-1 only groups (figure 4B–D). Conversely, anti-PD-1 treatment alone had no effect on CD8$^+$ T-cell infiltration into the tumor compared with PBS control mice, and tumors from vaccine +anti-PD-1 treated mice did not have more T cells than those receiving vaccine alone (figure 4B–D). Analysis of the P1A-specific CD8$^+$ TILs by tetramer staining showed that ChAdOx1/MVA P1A vaccination significantly increased both the percentage and total number of $P1A_{35\text{-}43}$ tetramer$^+$ cells in the TME (figure 4E–G). In numerical terms, this represented at least a 10-fold increase in numbers of $P1A_{35\text{-}43}$ tetramer$^+$ CD8$^+$ T cells in the tumor. We also analyzed tumor infiltration of both CD11b$^+$ Ly6C^{+hi} Lyg6G$^-$ and CD11b$^+$ Ly6C^{+int} Ly6G$^+$ cells, corresponding to monocytic myeloid-derived suppressor cell-like and granulocytic myeloid-derived suppressor cell-like phenotype, respectively,[32] but no significant difference was observed between different treatment groups (online supplemental figure S4).

Gene expression profiles (GEPs) in the 15V4T3 tumors following treatment were further assessed at the transcriptional level using RNA sequencing.

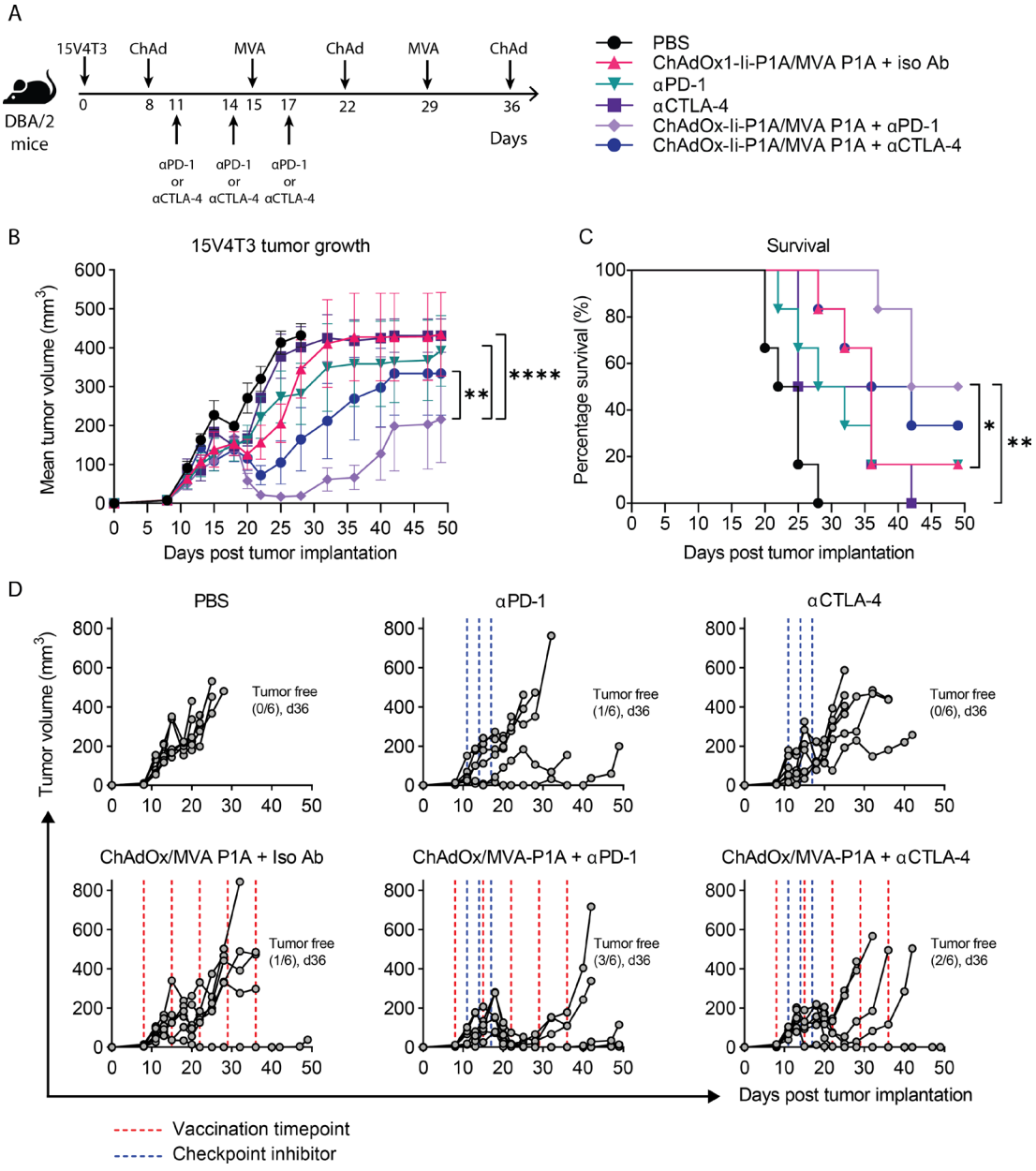

Figure 3 ChAdOx1/MVA P1A vaccination combined with immune checkpoint blockade enhances tumor control. (A) DBA/2 mice were implanted with 1x10^6 15V4T3 cells via s.c. injection. Eight days after tumor implantation, mice were randomized into experimental groupings according to tumor volume. Starting on day 8, mice then received vaccinations of 10^7 IU ChAdOx1-li-P1A / 10^6 PFU MVA-P1A alternating weekly or a PBS sham, and were treated with 3-doses of 100 µg anti-PD-1, anti-CTLA-4 or an isotype control antibody according to the schedule as shown. Tumor growth was followed for 50 days and mice were culled when tumor size reached size endpoints. (B-D) Mean tumor growth (B), survival curves (C) and individual tumor growth kinetics (D) for each group are shown. Tumor growth data in (B) are presented as mean tumor volume (mm^3) ± SEM. Each group contained 6 mice, with data representative of 2 independent experiments. Statistically significant differences in tumor volume between groups were determined by a two-way ANOVA followed by Tukey's post hoc test and statistical differences in survival data were determined by a log-rank test. *, p ≤ 0.05, **, p ≤ 0.01 ****, p ≤ 0.0001.

Differentially expressed genes (DEGs) were determined for each treatment group compared with the PBS control (online supplemental figure S5A), demonstrating that ChAdOx1/MVA P1A vaccination, either alone or combined with anti-PD-1, had a dramatic effect on tumor gene expression patterns (online supplemental figure S5B). Tumors from vaccinated mice had starkly different GEPs than those from groups not receiving vaccination (online supplemental figure S5C). Gene expression signatures associated with T-cell inflammation and IFN-γ response, which were shown to be predictive of clinical response to anti-PD-1 treatment,[21 33] were upregulated in the tumors of vaccinated mice (figure 4H). All samples from vaccinated mice had higher T-cell inflammation and IFN-γ response gene expression signature scores than unvaccinated

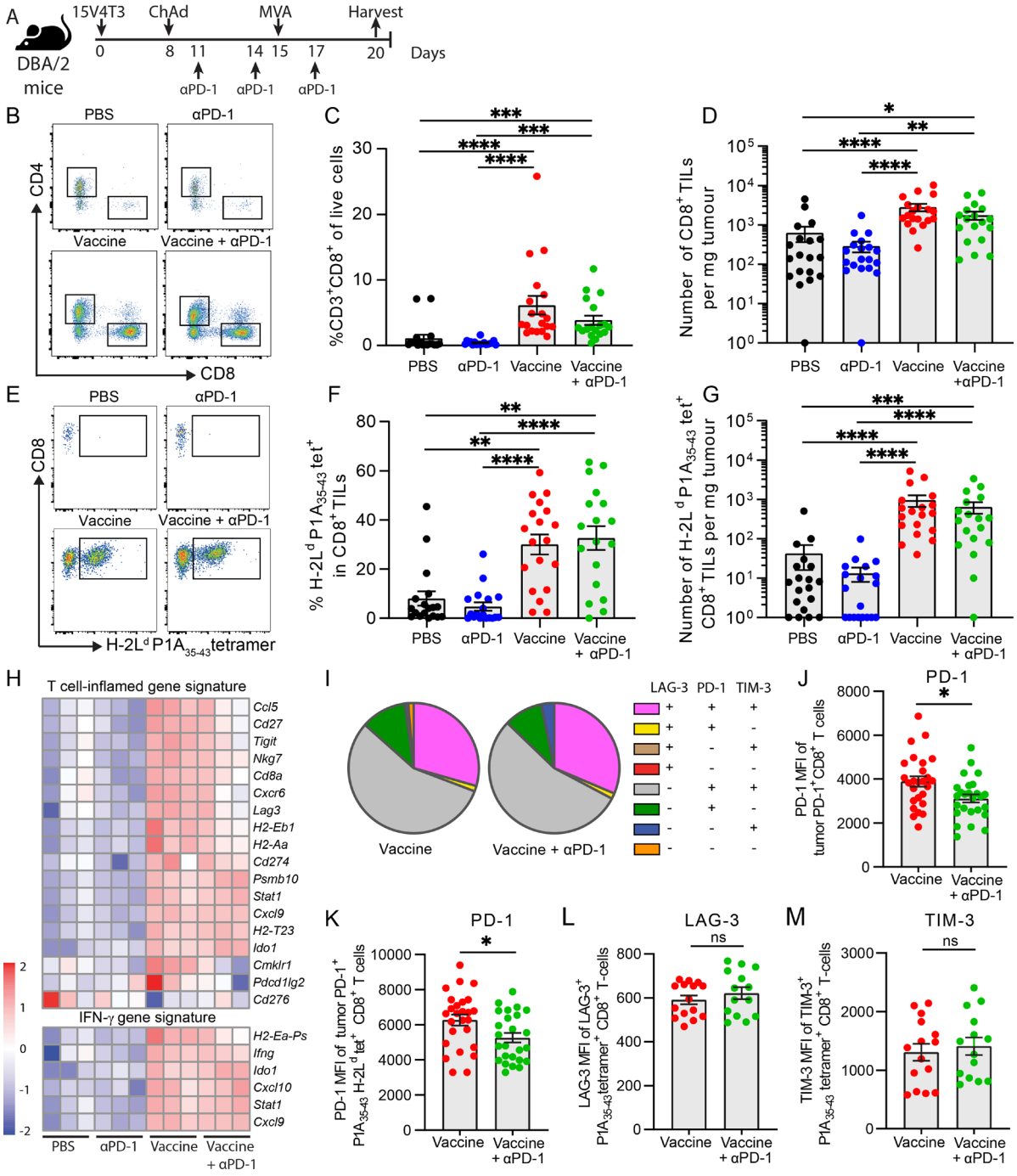

Figure 4 ChAdOx1/MVA P1A vaccination promotes CD8$^+$ T-cell infiltration into the TME. (A) DBA/2 mice were implanted with 1x10^6 15V4T3 cells via s.c. injection and treated with PBS control, ChAdOx-li-P1A (10^7 IU) /MVA-P1A (10^6 PFU), anti-PD-1 or combination treatment. Mice were sacrificed following treatment, and tumors surgically excised for analysis of immune cell infiltrate by flow cytometry. (B) Representative flow cytometry gating plots of CD8$^+$ TILs. (C) Percentage and (D) total numbers of CD8$^+$ TILs in 15V4T3 tumors, as quantified by flow cytometry. (E) Representative flow cytometry gating plots of P1A$_{35-43}$ tet$^+$ CD8$^+$ TILs. (F) Percentage and (G) total numbers of P1A$_{35-43}$ tet$^+$ CD8$^+$ TILs in 15V4T3 tumors, as quantified by flow cytometry. (H) RNA-sequencing analysis of tumor mRNA from 3 mice per group. Heatmaps showing log-CPM expression values of T-cell inflamed and IFN-γ gene expression signatures across all samples. Gene expression level has been scaled by Z-score, indicated by the heatmap color key. (I) Expression of PD-1, LAG-3 and TIM-3 receptors on tumor CD8$^+$ T cells from vaccine ± anti-PD-1 groups was evaluated by flow cytometry. Pie charts show the mean relative proportion of P1A-specific CD8$^+$ T cells expressing combinations of the receptors. (J) PD-1 mean fluorescence intensity (MFI) of tumor PD-1$^+$ CD8$^+$ TILs. (K) PD-1 MFI of PD-1$^+$ P1A$_{35-43}$ tet$^+$ CD8$^+$ TILs (L) LAG-3 MFI of LAG-3$^+$ P1A$_{35-43}$ tet$^+$ CD8$^+$ TILs. (M) TIM-3 MFI of TIM-3$^+$ P1A$_{35-43}$ tet$^+$ CD8$^+$ TILs. Tumor immune cell infiltrate data are shown as mean ± SEM. Each symbol represents an individual mouse, with 7-10 mice per group, pooled from 2-3 independent experiments. Statistically significant differences between multiple groups were determined by a Kruskal-Wallis test with Dunn's multiple comparisons test, between only two groups with a Mann-Whitney U test. *, p ≤ 0.05, **, p ≤ 0.01, ***, p ≤ 0.001, ****, p ≤ 0.0001.

mice (online supplemental figure S5D). Gene set variation analysis further confirmed tumors from vaccinated mice to be strongly enriched for expression of other previously established inflammatory and T-cell response gene sets (online supplemental figure S5E). In contrast to this, anti-PD-1 monotherapy had an insignificant effect on gene expression in the tumor, with no statistically significant DEGs identified (online supplemental figure S5A–C). Overexpression of proinflammatory factors *Ifng*, *Cxcl9*, *Cxcl10*, *Ccl3*, *Ccl5* and *Xcl1* in the tumors of vaccinated mice was further confirmed by RT-qPCR in a larger cohort of mice (online supplemental figure S6A), and by immunohistochemical staining for CCL5 and CXCL9, along with CD8 (online supplemental figure S6B).

We then further analyzed tumor-infiltrating $CD8^+$ T-cell phenotype by flow cytometry for expression of the negative immune checkpoint receptors PD-1, LAG-3 and TIM-3. High expression of these receptors was observed on tumor P1A-specific $CD8^+$ T cells, with the majority being $PD\text{-}1^+$ $TIM\text{-}3^+$ double positive, and a large fraction being $PD\text{-}1^+$ $TIM\text{-}3^+$ $LAG\text{-}3^+$ triple positive (figure 4I). We did not, however, detect much difference in the proportion between the two vaccinated groups. Interestingly, a reduction in the surface expression level of PD-1 on $CD8^+$ and P1A-specific $CD8^+$ TILs was observed in the tumors of the vaccine + anti-PD-1 combination group (figure 4J,K), but surface expression levels of LAG-3 and TIM-3 were not different (figure 4L,M). As PD-1 expression is also an indication of T-cell activation, it is hard to conclude that T cells from the combination group are less exhausted with less PD-1 expression. However, we found that almost 100% of P1A-specific $CD8^+$ T cells in the tumors in both groups express PD-1, indicating these are all activated T cells, and the ones with lower PD-1 expression in the combination group may have an advantage to overcome the negative PD-L1/PD-1 signaling in the TME,[34] especially given that 15V4T3 tumor cells expressed high levels of PD-L1 (online supplemental figure S3A–C).

Single-cell transcriptomic analysis of P1A-specific $CD8^+$ T cells identifies stem-like and effector gene signatures in the spleen and tumor

Next, we further characterized the vaccine-induced $P1A_{35\text{-}43}$-specific $CD8^+$ T cells from 15V4T3 tumor-bearing mice by single-cell RNA-sequencing (scRNA-seq) analysis. $P1A_{35\text{-}43}$ $tetramer^+$ cells from the spleens and tumors of mice receiving vaccine alone (referred to as spleen_vac and tumor_vac, respectively) and those receiving both vaccine and anti-PD-1 treatment (referred to as spleen_combi and tumor_combi, respectively) (figure 5A) were analyzed. Mice receiving anti-PD-1 only did not have P1A-specific $CD8^+$ T cells in sufficient numbers for analysis. Unsupervised clustering of single cells segregated cells into eight distinct clusters based on GEPs and were visualized by uniform manifold approximation and projection (UMAP), which broadly recapitulated two major cell states (figure 5B). Clusters 1 and 4 were referred to as 'stem-like' $CD8^+$ T-cell clusters as they primarily contained cells with upregulation of genes known to characterize a stem-like state such as *Tcf7*, *Sell* and *Lef1* (figure 5C and online supplemental figure S7). In contrast, clusters 0, 2, 3, 5, 6, and 7 were defined as 'effector' $CD8^+$ T-cell clusters, as they primarily contained cells with upregulation of genes encoding functional effector molecules such as *Gzmb* and *Ifng*, and those encoding inhibitory receptors such as *Tigit* and *Pdcd1* that are characteristic of highly activated but also potentially exhausted $CD8^+$ T cells (figure 5C and online supplemental figure S7).[35] K-nearest neighbor clustering data showed that the segregation of cells into different clusters was more strongly influenced by tissue of origin than anti-PD-1 treatment status (figure 5D). Major tissue-dependent differences were observed in terms of cluster proportion, with spleen having more stem-like cells than the tumor, while the majority of the tumor P1A-specific $CD8^+$ T cells were effector cells (figure 5E). Interestingly, we also observed spleen_combi to have a higher proportion of cells in the stem-like clusters compared with spleen_vac, whereas no noticeable difference in cluster composition was detected between tumor_combi and tumor_vac (figure 5E).

To further characterize the differentiation states of single cells from each condition, we constructed gene signatures that characterize each tissue/treatment setting using the DEGs between spleen_combi and spleen_vac, as well as those between tumor_combi and tumor_vac (online supplemental table S2), and measured their expression scores in each cell. Hierarchical clustering correlation analysis with stem-like and exhaustion T-cell signatures from other recent studies[36–41] (online supplemental table S3) showed an interesting association pattern. Gene signatures that were upregulated when comparing combination to vaccine treatment (SpleenCombi_vs_SpleenVac_UP and TumorCombi_vs_TumorVac_UP) were positively correlated with memory and stem-like T cell signatures associated with better ICB response,[36–39] while negatively correlated with exhausted and terminally differentiated T-cell signatures (figure 5F). On the other hand, the gene signatures upregulated in the vaccination-only group when comparing to the combination group (SpleenVac_vs_SpleenCombi_UP and TumorVac_vs_TumorCombi_UP) showed an opposite trend (figure 5F). In line with this observation, comparisons of characteristic stem-like and exhaustion markers between the two treatment groups showed a trend toward higher expression of stem-like markers in cells from spleen_combi than those from spleen_vac (figure 5G). Cells from tumor_combi exhibited a trend toward lower expression of most exhaustion markers compared with those from tumor_vac, despite the absence of a clear trend for the stem-like markers expressed between these two groups (figure 5G). Overall, these observations suggested that the combination of vaccination and anti-PD-1 treatment expanded the population of spleen P1A-specific stem-like $CD8^+$ T cells. As stem-like $CD8^+$ T cells represent the source of T cells that proliferate on PD-1 blockade,[42] this increased stem-like population of

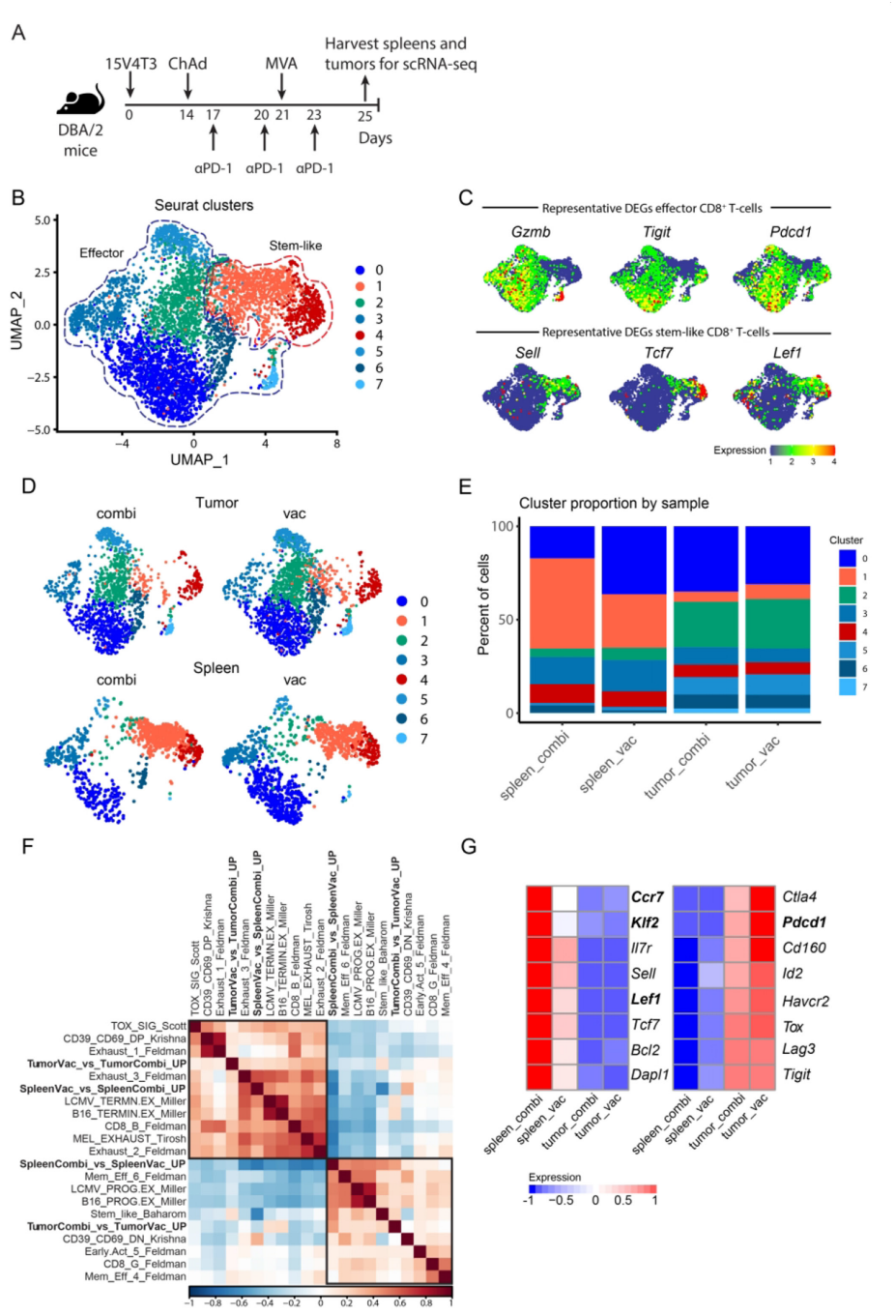

Figure 5 scRNA-seq analysis of P1A-specific CD8$^+$ T cells identifies stem-like and effector gene signatures in the spleen and tumor. (A) 15V4T3 tumor-bearing DBA/2 mice were vaccinated with ChAdOx1-li-P1A/MVA P1A ± anti-PD-1 treatment (n=10 per group). Tumors and spleens were collected on day 25 and P1A$_{35\text{-}43}$-specific CD8$^+$ T cells were isolated via H-2L^d P1A$_{35\text{-}43}$ tetramer staining and FACS. The transcriptional profile of P1A$_{35\text{-}43}$-specific CD8$^+$ T cells was determined via scRNA-seq using a 10X Genomics pipeline. (B) UMAP of P1A$_{35\text{-}43}$-specific CD8$^+$ T cells sorted from spleens and tumors, separated into eight clusters by k-nearest neighbor clustering analysis using Seurat. (C) UMAPs overlaid with representative DEGs in the effector (top) and stem-like clusters (bottom). (D) P1A$_{35\text{-}43}$-specific CD8$^+$ T cells cluster in distinct regions of the UMAP space based on their tissue of origin (tumor versus spleen) and treatment strategy (vaccination only versus vaccination combined with anti-PD-1 treatment). (E) Percentage of the eight Seurat clusters represented by each tissue type and treatment. (F) Clustered correlation matrix of exhausted and stem-like gene signatures from previously published data with those identified in combi- and vac-treated P1A$_{35\text{-}43}$-specific CD8$^+$ T cells from the spleen and tumor (TumorVac_vs_TumorCombi_UP, SpleenVac_vs_SpleenCombi_UP, SpleenCombi_vs_SpleenVac_UP, and TumorCombi_vs_TumorVac_UP). (G) Heatmap showing expression of characteristic stem-like (left) and exhaustion-related (right) genes by P1A-specific CD8$^+$ T cells in the spleen and tumor compared between vac and combi groups. Significantly differentially expressed genes are highlighted in bold for comparing spleen_combi vs spleen_vac (left panel) and tumor_combi vs tumor_vac (right panel), as determined with a Wilcoxon rank-sum test with Bonferroni correction. Color key indicates the z-scores of log-normalized expression.

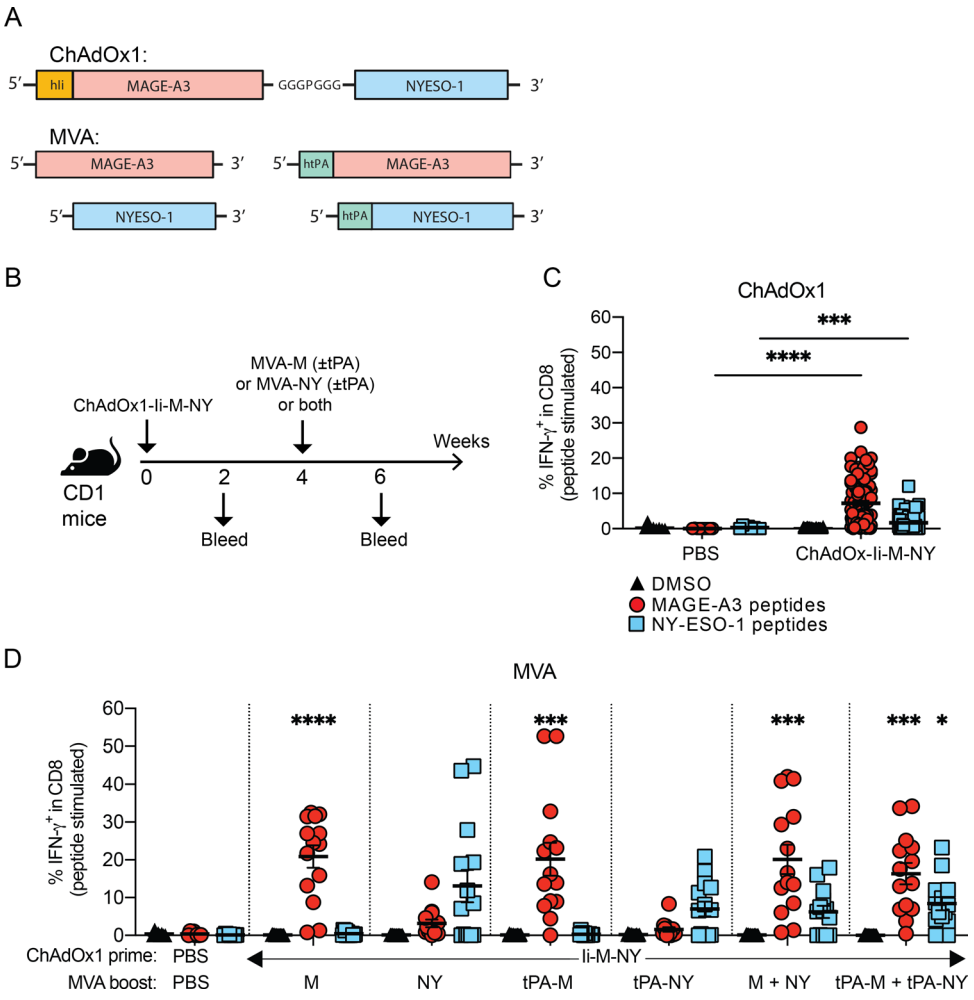

Figure 6 Evaluation of ChAdOx1/MVA prime-boost vaccination targeting MAGE-A3 and NY-ESO-1. (A) Design of ChAdOx1 and MVA vectors encoding the human MAGE-type antigens MAGE-A3 and NY-ESO-1. (B) CD1 outbred mice were vaccinated via i.m. injection according to the schedule shown. Mice received a prime vaccination with 10^8 IU of ChAdOx1-li-M-NY. Four weeks after ChAdOx1-M-NY, mice received a boost vaccination via a single injection with 10^7 PFU of either MVA-M (± tPA) or MVA-NY (± tPA), or two injections – one with 10^7 PFU of MVA-M (± tPA) and the other 10^7 PFU of MVA-NY (± tPA). To test the response to vaccination, mice were bled 16 days after ChAdOx1 and 14 days after MVA vaccinations. (C-D) Percentage of IFN-γ$^+$ CD8$^+$ T cells in the blood after (C) prime vaccination, (D) and the MVA boost vaccinations. PBMCs were stimulated ex vivo with 4 µg/ml of MAGE-A3 or NY-ESO-1 peptide pools, or a DMSO vehicle control. The percentage of antigen-specific IFN-γ$^+$ -producing CD8$^+$ T cells in the blood after each vaccination was determined by ICS and flow cytometry in response to stimulation with DMSO (black triangles), MAGE-A3 peptides (red circles) or NY-ESO-1 peptides (blue squares). Data are shown as the mean ± SEM and each symbol represents an individual mouse, with 8 mice in the PBS group and 14 mice per ChAdOx1/MVA vaccinated group, pooled from 2 independent experiments. Statistically significant difference is shown compared to the PBS control group and was determined by a Kruskal-Wallis test with Dunn's multiple comparisons test. *, p ≤ 0.05, **, p ≤ 0.01 ***, p ≤ 0.001, ****, p ≤ 0.0001.

tumor-specific CD8$^+$ T cells could contribute to explain the synergy between vaccine and anti-PD-1 for tumor control.

Evaluation of ChAdOx1/MVA prime-boost vaccination targeting MAGE-A3 and NY-ESO-1 for translation to the clinical setting

The therapeutic efficacy of ChAdOx1/MVA P1A vaccination in combination with anti-PD-1 against P1A-expressing tumors in mice suggests that ChAdOx1/MVA vaccination encoding MAGE-type antigens in combination with ICB has strong potential for translation to the clinic. Therefore, we developed ChAdOx1 and MVA vectors encoding the human MAGE-type antigens MAGE-A3 (M) and NY-ESO-1 (NY) (figure 6A). A dual-antigen fusion construct was inserted into the ChAdOx1 vector, with the two antigen coding sequences separated by a short polypeptide linker (GGGPGGG), and the TMB domain of human Ii fused to the N-terminus of MAGE-A3. MVA vectors were produced encoding only a single antigen, either MAGE-A3 or NY-ESO-1, with or without human tPA leader sequence (figure 6A). The immunogenicity of these vaccines was investigated using outbred CD1 mice (figure 6B). ChAdOx1-Ii-M-NY vaccination induced a significant increase of IFN-γ$^+$ CD8$^+$ T cells against both MAGE-A3 and NY-ESO-1 after prime

vaccination (figure 6C), and these CD8 responses further increased after an MVA boost (figure 6D). Mice given a boost vaccination with MVA-M had increased frequencies of MAGE-A3-specific CD8$^+$ T cells, while mice vaccinated with MVA-NY had increased frequencies of NY-ESO-1-specific CD8$^+$ T cells. Equally, vaccination with both MVA vectors (MVA-M and MVA-NY) simultaneously boosted the magnitude against both antigens. Again, inclusion of the tPA signal sequence via fusion to the N-terminus of the recombinant antigen encoded in the MVA vector was not found to significantly alter the magnitude of the antigen-specific CD8$^+$ T-cell response.

DISCUSSION

Positive clinical responses to ICB are limited to a minority of patients as most tumors are not sufficiently immunogenic to spontaneously prime antitumor CTLs.[1] Therapeutic cancer vaccines that induce de novo MAGE-type antigen-specific CTLs could improve ICB response rates in patients with MAGE$^+$ tumors. As compared with neoantigens, MAGE-type antigens are likely less immunogenic, so it is crucial to use a vaccine platform that can induce a strong CD8 response. Here, we evaluated the viral vector ChAdOx1/MVA vaccination regimen in the murine setting using the tumor antigen P1A, the best-known murine equivalent of human MAGE-type antigens. Our results indicate that ChAdOx1/MVA P1A vaccination induces a high magnitude multifunctional P1A-specific CD8$^+$ T-cell response in DBA/2 mice, which has not been observed in previous studies when P1A was delivered in other vaccine platforms,[43] except using arenavirus vector.[44] The induced CD8 response is also comparable to those against other tumor antigens delivered by ChAdOx1/MVA vaccination.[30] The magnitude of the CD8 response can be further enhanced by tethering the Ii-TMD sequence to the N-terminus of P1A encoded in ChAdOx1, corroborating earlier findings showing benefits of linking the transgene to Ii in adenoviral vectors.[27]

It has recently become clear that a CD8$^+$ T cell-inflamed or 'hot' TME underlies a positive clinical response to ICB.[7 22] Tumors obtained after implantation of 15V4T3 cells appear as 'cold' tumors that are largely devoid of CD8$^+$ T cells. However, ChAdOx1/MVA P1A vaccination, either alone or in combination with anti-PD-1 dramatically increased the density of CD8$^+$ T-cells and number of P1A-specific CD8$^+$ T cells in the TME. Although ChAdOx1/MVA vaccination was reported to induce strong antigen-specific CD8$^+$ T-cell responses,[30] its effect on tumor immune infiltration had not been studied. Our results demonstrate that ChAdOx1/MVA P1A vaccination enhances CD8$^+$ T cells levels in poorly infiltrated tumors, and improves response to anti-PD-1 treatment. Vaccination also induces characteristic gene expression signatures of T-cell inflammation and IFN-γ-response, which are the strongest predictors of positive response to anti-PD-1 blockade in clinical studies.[21 33] Genes that were overexpressed in tumors from vaccinated mice included IFN-γ inducible T-cell chemokines such as *Cxcl9* and *Cxcl10*, which are key mediators regulating CD8$^+$ T-cell recruitment in tumors.[45–47] Increased chemokine expression suggests that ChAdOx1/MVA vaccination generates conditions in the tumor that drive CD8$^+$ T-cell recruitment and inflammation.

When combined with anti-PD-1, the vaccine showed a drastically improved therapeutic efficacy. Tumors from mice receiving the combination did not show increased numbers of vaccine-induced infiltrating CD8$^+$ T cells, but these cells expressed less PD-1 at their surface, suggesting they might be less exhausted, even though they expressed similar levels of LAG-3 and TIM-3. scRNA-seq analysis of $P1A_{35-43}$-specific CD8$^+$ T cells revealed important differences with regard to stem-like vaccine-induced CD8$^+$ T cells, whose proportion was higher in the spleen of mice receiving the combination as compared with vaccine alone. Stem-like CD8$^+$ T cells have been described as a reservoir of less-differentiated CD8$^+$ T cells without effector function but with proliferative potential, which can differentiate into mature effector cells.[48] They are usually located in secondary lymph nodes or tertiary lymphoid structures.[48 49] Stem-like CD8$^+$ T cells mostly develop on chronic antigenic stimulation, and represent a self-renewed source of effector CD8$^+$ T cells, which can populate non-lymphoid tissues, including tumors.[42] Their transition into effector CD8$^+$ T cells is stimulated by PD-1 blockade, and as such they provide the proliferative burst of CD8$^+$ T cells that is observed during anti-PD-1 therapy and mediates tumor rejection.[42 50] It is possible that the better antitumor efficacy we observed with the combination treatment results from this increased stem-like CD8$^+$ T cell population, acting as a reservoir to continuously produce effector P1A-specific CD8$^+$ T cells that can then migrate to the tumor. Such a synergistic mechanism would be in line with recent observations showing that a vaccine modality inducing more stem-like CD8$^+$ T cells induced better tumor rejection on PD-1 blockade.[41] However, further studies will be needed to confirm this mechanism in our model.

To support clinical development of our strategy, we evaluated a ChAdOx1/MVA MAGE-A3-NY-ESO-1 in outbred CD1 mice. Though the MAGE-A3 and NY-ESO-1 antigens are xenogeneic in CD1 mice and thus recognized as foreign by the CD1 immune system, it is still useful to validate and demonstrate some key features of the ChAdOx1/MVA MAGE-A3-NY-ESO-1 vaccination strategy. Our results demonstrate that a 'dual antigen prime' with ChAdOx1 encoding both antigens, and a 'single antigen boost' approach with MVA encoding a single antigen could generate very high antigen-specific CD8$^+$ T-cell responses of up to 50% of CD8$^+$ T cells in the blood in some mice. Crucially, we found that the specificity and direction of the response could be tightly controlled by varying the antigen encoded in the MVA

boost after the dual antigen prime. As MAGE-type antigens are expressed differentially in tumors,[9] this strategy allows for preferential targeting of the particular antigens expressed by an individual patient's tumor.

In conclusion, we have shown that ChAdOx1/MVA MAGE vaccination induces potent MAGE-specific CTL responses, promotes $CD8^+$ T-cell infiltration in the tumor site and expression of clinically important gene signatures, and improves response to ICB therapy. With these promising data, we will evaluate this cancer vaccine strategy in a clinical trial that will commence shortly.

Author affiliations
[1]Ludwig Institute for Cancer Research, Nuffield Department of Medicine, University of Oxford, Oxford, UK
[2]Département Biologie, Université Claude Bernard Lyon 1, Villeurbanne, Auvergne-Rhône-Alpes, France
[3]Department of Gastroenterology, Peking Union Medical College Hospital, Beijing, China
[4]The Jenner Institute, Nuffield Department of Medicine, University of oxford, Oxford, UK
[5]Ludwig Institute for Cancer Research, WELBIO, de Duve Institute, UCLouvain, Brussels, Belgium

Acknowledgements We thank V. Clark and H. Gray for animal husbandry, and F. Howe, M. Muers and Xiao Qin for critical manuscript reading.

Contributors IR, AVSH, CSKL and BJVdE conceived the experiments. JM, CSKL and BJVdE designed the experiments. IR and CSKL designed the viral vectors. CSKL and EP generated all viral vector constructs and IR supervised the viral vectors construction. JM, LN, RAR-V, VP-A, YZ, FC and CSKL performed the experiments. JM, HFC, RAR-V and CSKL analyzed the data. JM, CSKL and BJVdE wrote the manuscript.

Funding This work was supported by Ludwig Cancer Research and CRUK Oxford Center Development Fund (CRUKDF 0216-BVDE) to BJVdE. and IR. VP-A was registered in the EMJMD LIVE (Erasmus+ Mundus Joint Master Degree Leading International Vaccinology Education), cofunded by the EACEA (Education, Audiovisual and Culture Executive Agency, award 2015-2323) of the European commission, and received a scholarship from the EACEA. CSKL was supported by a fellowship from Swiss National Science Foundation (P300P3_155374).

Competing interests IR, AVSH, CSKL, and BJVdE are inventors on a patent that covers viral vectors and methods for the prevention and treatment of cancer. AVSH is a cofounder of and shareholder in Vaccitech Ltd which has supported the MAGE cancer vaccine program and has licensed rights to the ChAdOx1-MVA platform in cancer.

Patient consent for publication Not required.

Ethics approval All animal work was approved by the University of Oxford Animal Care and Ethical Review Committee and experimental procedures were carried out in accordance with the terms of the UK Animals (Scientific Procedures) Act Project Licenses P0D369534 and PB050649E.

Provenance and peer review Not commissioned; externally peer reviewed.

Data availability statement Data are available in a public, open access repository. The gene expression data generated in this study are available at GEO: GSE181111 and GSE181183. The rest of the data are in the Mendeley dataset with DOI: 10.17632/h6rcgfrwry.1

ORCID iDs
Carol Sze Ki Leung http://orcid.org/0000-0002-1545-7228
Benoit J Van den Eynde http://orcid.org/0000-0002-4995-3270

REFERENCES

1 Ribas A, Wolchok JD. Cancer immunotherapy using checkpoint blockade. *Science* 2018;359:1350–5.
2 Hargadon KM, Johnson CE, Williams CJ. Immune checkpoint blockade therapy for cancer: an overview of FDA-approved immune checkpoint inhibitors. *Int Immunopharmacol* 2018;62:29–39.
3 Spranger S, Koblish HK, Horton B, *et al*. Mechanism of tumor rejection with doublets of CTLA-4, PD-1/PD-L1, or IDO blockade involves restored IL-2 production and proliferation of CD8(+) T cells directly within the tumor microenvironment. *J Immunother Cancer* 2014;2:3.
4 Larkin J, Chiarion-Sileni V, Gonzalez R, *et al*. Five-Year survival with combined nivolumab and ipilimumab in advanced melanoma. *N Engl J Med* 2019;381:1535–46.
5 Gandhi L, Rodríguez-Abreu D, Gadgeel S, *et al*. Pembrolizumab plus chemotherapy in metastatic non-small-cell lung cancer. *N Engl J Med* 2018;378:2078–92.
6 Motzer RJ, Tannir NM, McDermott DF, *et al*. Nivolumab plus ipilimumab versus sunitinib in advanced renal-cell carcinoma. *N Engl J Med* 2018;378:1277–90.
7 Tumeh PC, Harview CL, Yearley JH, *et al*. Pd-1 blockade induces responses by inhibiting adaptive immune resistance. *Nature* 2014;515:568–71.
8 Massarelli E, William W, Johnson F, *et al*. Combining immune checkpoint blockade and tumor-specific vaccine for patients with incurable human papillomavirus 16-related cancer: a phase 2 clinical trial. *JAMA Oncol* 2019;5:67–73.
9 Coulie PG, Van den Eynde BJ, van der Bruggen P, *et al*. Tumour antigens recognized by T lymphocytes: at the core of cancer immunotherapy. *Nat Rev Cancer* 2014;14:135–46.
10 Yuan J, Adamow M, Ginsberg BA, *et al*. Integrated NY-ESO-1 antibody and CD8+ T-cell responses correlate with clinical benefit in advanced melanoma patients treated with ipilimumab. *Proc Natl Acad Sci U S A* 2011;108:16723–8.
11 Olsen LR, Tongchusak S, Lin H, *et al*. TANTIGEN: a comprehensive database of tumor T cell antigens. *Cancer Immunol Immunother* 2017;66:731–5.
12 Zhang G, Chitkushev L, Olsen LR, *et al*. TANTIGEN 2.0: a knowledge base of tumor T cell antigens and epitopes. *BMC Bioinformatics* 2021;22:40.
13 Vansteenkiste JF, Cho BC, Vanakesa T, *et al*. Efficacy of the MAGE-A3 cancer immunotherapeutic as adjuvant therapy in patients with resected MAGE-A3-positive non-small-cell lung cancer (MAGRIT): a randomised, double-blind, placebo-controlled, phase 3 trial. *Lancet Oncol* 2016;17:822–35.
14 Dreno B, Thompson JF, Smithers BM, *et al*. Mage-A3 immunotherapeutic as adjuvant therapy for patients with resected, MAGE-A3-positive, stage III melanoma (DERMA): a double-blind, randomised, placebo-controlled, phase 3 trial. *Lancet Oncol* 2018;19:916–29.
15 Brichard VG, Godechal Q. MAGE-A3-specific anticancer immunotherapy in the clinical practice. *Oncoimmunology* 2013;2:e25995.
16 Kruit WHJ, Suciu S, Dreno B, *et al*. Selection of immunostimulant AS15 for active immunization with MAGE-A3 protein: results of a randomized phase II study of the European organisation for research and treatment of cancer melanoma group in metastatic melanoma. *J Clin Oncol* 2013;31:2413–20.
17 Ewer KJ, Lambe T, Rollier CS, *et al*. Viral vectors as vaccine platforms: from immunogenicity to impact. *Curr Opin Immunol* 2016;41:47–54.
18 Antrobus RD, Coughlan L, Berthoud TK, *et al*. Clinical assessment of a novel recombinant simian adenovirus ChAdOx1 as a vectored vaccine expressing conserved influenza A antigens. *Mol Ther* 2014;22:668–74.
19 Cappuccini F, Bryant R, Pollock E, *et al*. Safety and immunogenicity of novel 5T4 viral vectored vaccination regimens in early stage

prostate cancer: a phase I clinical trial. *J Immunother Cancer* 2020;8:e000928.
20 Rühl J, Citterio C, Engelmann C, *et al*. Heterologous prime-boost vaccination protects against EBV antigen-expressing lymphomas. *J Clin Invest* 2019;129:2071–87.
21 Ayers M, Lunceford J, Nebozhyn M, *et al*. IFN-γ-related mRNA profile predicts clinical response to PD-1 blockade. *J Clin Invest* 2017;127:2930–40.
22 Lee JS, Ruppin E. Multiomics prediction of response rates to therapies to inhibit programmed cell death 1 and programmed cell death 1 ligand 1. *JAMA Oncol* 2019;5:1614–8.
23 Brändle D, Bilsborough J, Rülicke T, *et al*. The shared tumor-specific antigen encoded by mouse gene P1A is a target not only for cytolytic T lymphocytes but also for tumor rejection. *Eur J Immunol* 1998;28:4010–9.
24 Uyttenhove C, Godfraind C, Lethé B, *et al*. The expression of mouse gene P1A in testis does not prevent safe induction of cytolytic T cells against a P1A-encoded tumor antigen. *Int J Cancer* 1997;70:349–56.
25 Boon T, Van den Eynde B, Hirsch H, *et al*. Genes coding for tumor-specific rejection antigens. *Cold Spring Harb Symp Quant Biol* 1994;59:617–22.
26 Leung CS, Maurer MA, Meixlsperger S, *et al*. Robust T-cell stimulation by Epstein-Barr virus-transformed B cells after antigen targeting to DEC-205. *Blood* 2013;121:1584–94.
27 Halbroth BR, Sebastian S, Poyntz HC, *et al*. Development of a Molecular Adjuvant to Enhance Antigen-Specific $CD8^+$ T Cell Responses. *Sci Rep* 2018;8:15020.
28 Biswas S, Dicks MDJ, Long CA, *et al*. Transgene optimization, immunogenicity and in vitro efficacy of viral vectored vaccines expressing two alleles of Plasmodium falciparum AMA1. *PLoS One* 2011;6:e20977.
29 Van den Eynde B, Lethé B, Van Pel A, *et al*. The gene coding for a major tumor rejection antigen of tumor P815 is identical to the normal gene of syngeneic DBA/2 mice. *J Exp Med* 1991;173:1373–84.
30 Cappuccini F, Stribbling S, Pollock E, *et al*. Immunogenicity and efficacy of the novel cancer vaccine based on simian adenovirus and MVA vectors alone and in combination with PD-1 mAb in a mouse model of prostate cancer. *Cancer Immunol Immunother* 2016;65:701–13.
31 Mosely SIS, Prime JE, Sainson RCA, *et al*. Rational selection of syngeneic preclinical tumor models for immunotherapeutic drug discovery. *Cancer Immunol Res* 2017;5:29–41.
32 Youn J-I, Kumar V, Collazo M, *et al*. Epigenetic silencing of retinoblastoma gene regulates pathologic differentiation of myeloid cells in cancer. *Nat Immunol* 2013;14:211–20.
33 Cristescu R, Mogg R, Ayers M, *et al*. Pan-tumor genomic biomarkers for PD-1 checkpoint blockade-based immunotherapy. *Science* 2018;362:eaar3593.
34 Juneja VR, McGuire KA, Manguso RT, *et al*. Pd-L1 on tumor cells is sufficient for immune evasion in immunogenic tumors and inhibits CD8 T cell cytotoxicity. *J Exp Med* 2017;214:895–904.
35 Wherry EJ, Kurachi M. Molecular and cellular insights into T cell exhaustion. *Nat Rev Immunol* 2015;15:486–99.
36 Tirosh I, Izar B, Prakadan SM, *et al*. Dissecting the multicellular ecosystem of metastatic melanoma by single-cell RNA-seq. *Science* 2016;352:189–96.
37 Scott AC, Dündar F, Zumbo P, *et al*. Tox is a critical regulator of tumour-specific T cell differentiation. *Nature* 2019;571:270–4.
38 Miller BC, Sen DR, Al Abosy R, *et al*. Subsets of exhausted $CD8^+$ T cells differentially mediate tumor control and respond to checkpoint blockade. *Nat Immunol* 2019;20:326–36.
39 Sade-Feldman M, Yizhak K, Bjorgaard SL, *et al*. Defining T cell states associated with response to checkpoint immunotherapy in melanoma. *Cell* 2018;175:e20:998–1013.
40 Krishna S, Lowery FJ, Copeland AR, *et al*. Stem-Like CD8 T cells mediate response of adoptive cell immunotherapy against human cancer. *Science* 2020;370:1328–34.
41 Baharom F, Ramirez-Valdez RA, Tobin KKS, *et al*. Intravenous nanoparticle vaccination generates stem-like $TCF1^+$ neoantigen-specific $CD8^+$ T cells. *Nat Immunol* 2021;22:41–52.
42 Im SJ, Hashimoto M, Gerner MY, *et al*. Defining CD8+ T cells that provide the proliferative burst after PD-1 therapy. *Nature* 2016;537:417–21.
43 Näslund TI, Uyttenhove C, Nordström EKL, *et al*. Comparative prime-boost vaccinations using Semliki Forest virus, adenovirus, and ALVAC vectors demonstrate differences in the generation of a protective central memory CTL response against the P815 tumor. *J Immunol* 2007;178:6761–9.
44 Bonilla WV, Kirchhammer N, Marx A-F, *et al*. Heterologous arenavirus vector prime-boost overrules self-tolerance for efficient tumor-specific CD8 T cell attack. *Cell Rep Med* 2021;2:100209.
45 Harlin H, Meng Y, Peterson AC, *et al*. Chemokine expression in melanoma metastases associated with CD8+ T-cell recruitment. *Cancer Res* 2009;69:3077–85.
46 Mikucki ME, Fisher DT, Matsuzaki J, *et al*. Non-Redundant requirement for CXCR3 signalling during tumoricidal T-cell trafficking across tumour vascular checkpoints. *Nat Commun* 2015;6:7458.
47 Romero JM, Grünwald B, Jang G-H, *et al*. A Four-Chemokine signature is associated with a T-cell-Inflamed phenotype in primary and metastatic pancreatic cancer. *Clin Cancer Res* 2020;26:1997–2010.
48 Im SJ, Konieczny BT, Hudson WH, *et al*. PD-1+ stemlike CD8 T cells are resident in lymphoid tissues during persistent LCMV infection. *Proc Natl Acad Sci U S A* 2020;117:4292–9.
49 Lugli E, Dominguez MH, Gattinoni L, *et al*. Superior T memory stem cell persistence supports long-lived T cell memory. *J Clin Invest* 2013;123:594–9.
50 Siddiqui I, Schaeuble K, Chennupati V, *et al*. Intratumoral $Tcf1^+PD\text{-}1^+CD8^+$ T Cells with Stem-like Properties Promote Tumor Control in Response to Vaccination and Checkpoint Blockade Immunotherapy. *Immunity* 2019;50:e10:195–211.

Supplemental materials and methods

Viral vectors

The coding sequence of P1A or the juxtaposed coding sequences of MAGE-A3 and NY-ESO-1 were inserted into the E1 locus of ChAdOx1 under a CMV immediate early promoter. A sequence coding for the 26 amino acid transmembrane domain of the MHC-II invariant chain with sequence fragment was linked to the N terminus of the transgene, described previously [1]. The MVA vectors encoding P1A, MAGE-A3 and NY-ESO-1 were constructed with or without the leader sequence of the human tissue plasminogen activator gene (tPA) with the F11 promoter driving transgene expression. Viral vectors were isolated and purified as described [2] . The purity and identity of the viral vectors were confirmed by PCR.

Tumor biopsy for gene expression analysis

Tumor masses were surgically excised and pieces ≤30 mg were immediately frozen in liquid nitrogen and stored at minus 80°C. Total cellular RNA was isolated using a RNeasy mini kit (Qiagen) with column-based RNase-free DNase I (Qiagen) digestion to remove genomic DNA, then used for gene expression analysis.

Reverse Transcription Quantitative PCR (RT-qPCR)

Total cellular RNA (0.5 µg) was used to synthesize first single-strand cDNA using the SuperScript III First-Strand Synthesis kit (Thermo Fisher). Reactions were performed according to the manufacturer's protocol. For quantification of cDNA by qPCR, the QuantiTect SYBR Green PCR kit (Qiagen) was used and reactions set up according to the manufacturer's instructions. Reactions were run on the StepOnePlus™ Real-Time PCR System (Applied Biosystems) at the following conditions – 95°C - 15 min, (94°C 15s + 60°C 30s + 72°C 30s) x 40 cycles. Gene expression at the mRNA level for each target gene assayed was quantified relative to an internal housekeeping gene control. The housekeeping genes

used were either *ActB* or *Hprt1*. To determine relative mRNA expression, the mean ΔCt (difference in cycle threshold number) was calculated for each target gene relative to *ActB* or *Hprt1*. ΔCt for a given target gene in each sample was therefore calculated according to the formula ΔCt = Ct Target gene – Ct Housekeeping gene. Relative mRNA expression data are shown as $2^{-\Delta Ct}$. The list of primers used is shown in table S1.

Table S1: qPCR primer sequences

Primer	Sequence (5'-3')
Actb for	CCTTCAACACCCCAGCCATGTA
Actb rev	GGATGGCGTGAGGGAGAGCAT
P1A for	AGCTGAGGAAATGGGTGCTG
P1A rev	CAGCATTTTCACACCTACACTCCA
Hprt1 for	AGTGTTGGATACAGGCCAGAC
Hprt1 rev	CGTGATTCAAATCCCTGAAGT
Cxcl9 for	GCCATGAAGTCCGCTGTTCT
Cxcl9 rev	GGGTTCCTCGAACTCCACACT
Cxcl10 for	GACGGTCCGCTGCAACTG
Cxcl10 rev	GCTTCCCTATGGCCCTCATT
Ccl3 for	GCCAGGTGTCATTTTCCTGACTA
Ccl3 rev	AGGCATTCAGTTCCAGGTCA
Ccl5 for	GCAAGTGCTCCAATCTTGCA
Ccl5 rev	CTTCTCTGGGTTGGCACACA
Ifng for	CGGCACAGTCATTGAAAGCCTA
Ifng rev	GTTGCTGATGGCCTGATTGTC
Xcl1 for	CTTTCCTGGGAGTCTGCTGC
Xcl1 Rev	CAGCCGCTGGGTTTGTAAGT

Immunohistochemistry

Tumor tissue was fixed and embedded in paraffin. Tissue slices of 4 µm were rehydrated in a series of histo-clear and graded ethanol. The tissue sections were incubated at 95 °C with citrate buffer (pH 6) for antigen retrieval and blocked with 1 µg/mL Rat IgG (Vector Lab) diluted into 2.5 % Normal Goat Serum (Vector Labs) before staining with rabbit polyclonal anti-CD8a (361003, Synaptic Systems), anti-CCL5 (clone 25H14L17, ThermoFisher) or anti-CXCL9 (clone 11H1L14, ThermoFisher). Then the slides were washed and were incubated with ImmPRESS HRP Reagent peroxidase Anti-Rabbit IgG (Vector Labs). The sections were developed using ImmPACT DAB Chromogen (Vector Labs) and stained with haematoxylin,

dehydrated in a graded series of ethanol and histo-clear and cover slipped. Immunostaining were imaged using NanoZoomer S210 Digital slide scanner.

Bulk RNA-sequencing data analysis

Fastq sequencing data files were trimmed of adapter sequences using Skewer [3] and reads mapped to mouse genome GRCm38.ERCC using HISAT2 aligner [4]. A count matrix reporting the numbers of reads mapping to each gene was generated using the featureCounts program in the Subread UNIX package [5] and gene expression was calculated as counts per million (CPM). Genes expressed at a level <1 CPM were excluded from further analysis. R package "edgeR" was used for data normalization and differential expression analysis [6]. Briefly, count data was normalized using the trimmed mean of M values (TMM) method and differential gene expression analysis between indicated samples determined using the glmQLFTest method. The Benjamini–Hochberg correction was applied to the list of differentially expressed genes to calculate corrected P-values (P_{adj}). Genes with a $P_{adj} < 0.05$ and an absolute $\log_2FC > 1$ were considered as differentially expressed. T-cell inflamed and IFN-γ-related mRNA gene expression signatures were defined and associated gene expression signature scores calculated as described by M. Ayers and colleagues [7]. Heatmaps showing logCPM gene expression values from TMM-normalized count data were generated using the pheatmap R package. Gene set variation analysis (GSVA) was performed using R package GSVA [8]. The gene ontology (GO) gene sets used were obtained from the Molecular Signatures Database [9]. Hierarchical clustering and heatmap visualization of the GSVA matrix was performed using R package pheatmap.

Single-cell RNA-sequencing (scRNA-seq) data analysis

scRNA-seq data were pre-processed using the 10x Genomics CellRanger at the Oxford Genomics Centre and further analyzed with the R package Seurat v3.1.4 [10]. For spleen

samples, cells with less than 200 UMI or detected genes were filtered out. For tumor samples, cells with UMI less than 500 or detected genes less than 300 were filtered out. For both types of samples, cells with higher than 10 percent of transcripts mapping to mitochondrial gene were filtered out. In addition, 100 potential doublets were removed using R package scDblFinder v1.3.0 [11]. Finally, genes expressed in less than 5 cells were removed, leading to a total of 5,578 cells and 11,502 genes for analysis. SCTransform was used to normalize samples, regress out cell cycle differences and identify highly variable genes. Mitochondrial, cell cycle, ribosomal and pseudo genes were excluded from the variable genes and the top 2000 most variable genes were used for sample integration using Seurat's integration workflow. Prior to clustering, principal component analysis (PCA) was applied to the variable genes of the dataset to reduce dimensionality. The top 25 principal components were used for Seurat's K-nearest neighbor (KNN) graph-based clustering analysis and the resulting clusters were visualized using the Uniform Manifold Approximation and Projection (UMAP). Differential gene expression analysis was performed on the log-normalized data with Seurat v4.0.1 by the non-parametric Wilcoxon rank-sum test using the FindMarkers function followed by Bonferroni correction using all genes for adjusted p-value calculation. Top DEGs were visualized using ComplexHeatmap ver2.6.2. Gene signatures characterizing the four experimental groups were generated by using the DEGs, with an adjusted p-value < 0.01 and average log2 fold change > 0.25, between combination therapy-treated and vaccine-treated single $P1A_{35-43}$-specific $CD8^+$ T cells in the spleen and tumor, respectively. For single-cell gene signature scoring, log-normalized data was used as input with gene signature lists (Table S2), which include the four above-mentioned gene signatures, as well as stem-like and exhaustion signatures from other recent studies. Signature scores for all gene signatures were calculated using the

AddModuleScore function in Seurat followed by z-scale normalization for cross-signature comparison across cells. Clustered correlation matrix showing the Pearson correlation coefficients between various gene signatures from single $P1A_{35-43}$-specific $CD8^+$ T cells was generated using R package Corrplot v0.84 and visualized after hierarchical clustering. Seurat's AverageExpression function was used to calculate the average expression of genes for each experimental group. Heatmaps were plotted using R package pheatmap v1.0.12.

References

1. Halbroth BR, Sebastian S, Poyntz HC*, et al.* Development of a Molecular Adjuvant to Enhance Antigen-Specific CD8(+) T Cell Responses. *Sci Rep* 2018;8:15020.
2. Dicks MD, Spencer AJ, Edwards NJ*, et al.* A novel chimpanzee adenovirus vector with low human seroprevalence: improved systems for vector derivation and comparative immunogenicity. *PLoS One* 2012;7:e40385.
3. Jiang H, Lei R, Ding SW*, et al.* Skewer: a fast and accurate adapter trimmer for next-generation sequencing paired-end reads. *BMC Bioinformatics* 2014;15:182.
4. Kim D, Langmead B, Salzberg SL. HISAT: a fast spliced aligner with low memory requirements. *Nat Methods* 2015;12:357-60.
5. Liao Y, Smyth GK, Shi W. featureCounts: an efficient general purpose program for assigning sequence reads to genomic features. *Bioinformatics* 2014;30:923-30.
6. Robinson MD, McCarthy DJ, Smyth GK. edgeR: a Bioconductor package for differential expression analysis of digital gene expression data. *Bioinformatics* 2010;26:139-40.
7. Ayers M, Lunceford J, Nebozhyn M*, et al.* IFN-gamma-related mRNA profile predicts clinical response to PD-1 blockade. *J Clin Invest* 2017;127:2930-40.

8. Hanzelmann S, Castelo R, Guinney J. GSVA: gene set variation analysis for microarray and RNA-seq data. *BMC Bioinformatics* 2013;14:7.

9. Liberzon A, Subramanian A, Pinchback R*, et al.* Molecular signatures database (MSigDB) 3.0. *Bioinformatics* 2011;27:1739-40.

10. Stuart T, Butler A, Hoffman P*, et al.* Comprehensive Integration of Single-Cell Data. *Cell* 2019;177:1888-902 e21.

11. Germain PL, Sonrel A, Robinson MD. pipeComp, a general framework for the evaluation of computational pipelines, reveals performant single cell RNA-seq preprocessing tools. *Genome Biol* 2020;21:227.

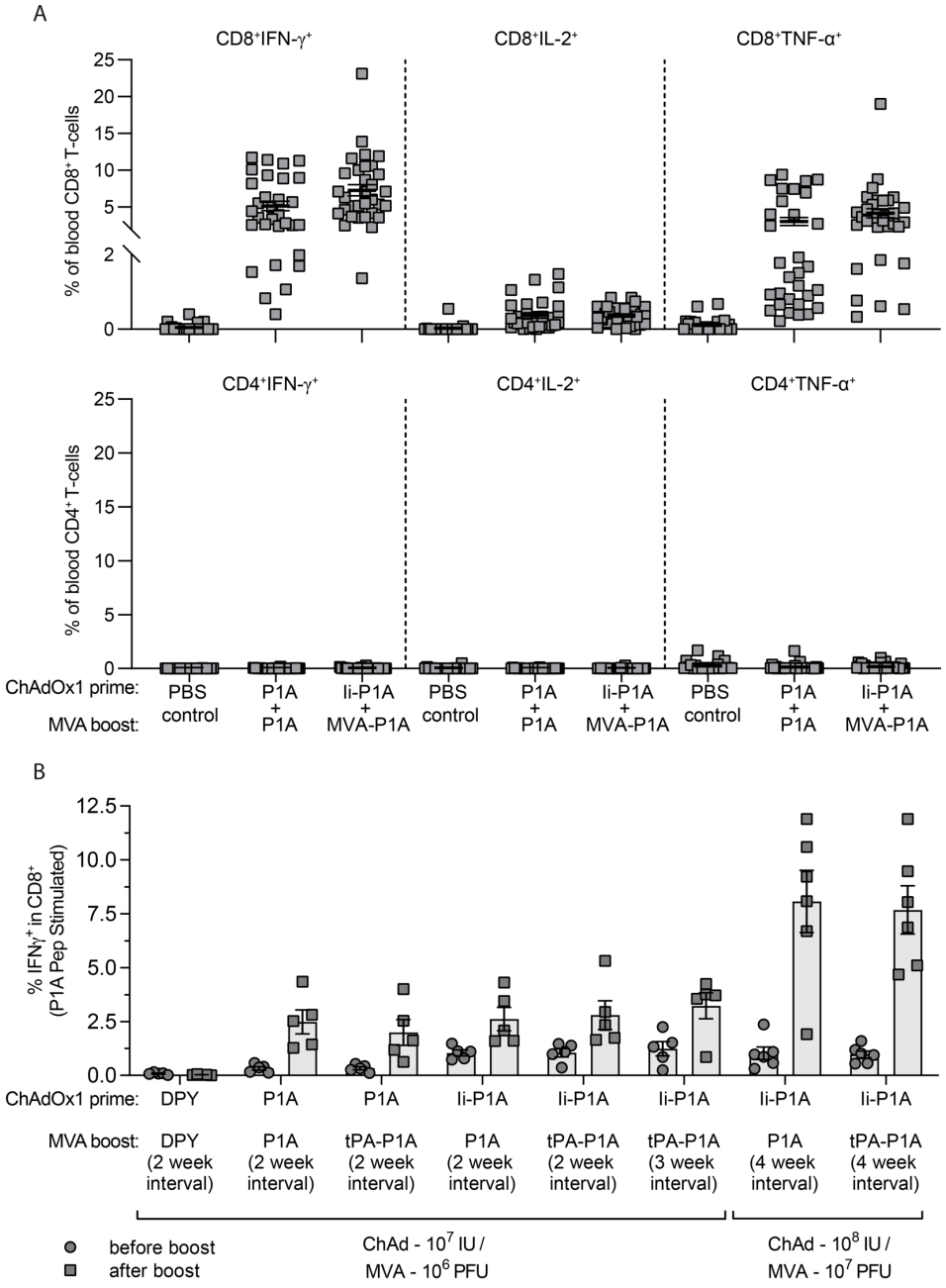

Figure S1: Blood P1A-specific T-cell responses induced by ChAdOx1/MVA P1A vaccination schemes. (A) DBA/2 mice received ChAdOx1-P1A (± Ii) and MVA-P1A vaccinations 4 weeks apart, and were bled after MVA vaccination as described in Fig. 1. PBMCs were stimulated *ex vivo* with 4 µg/ml of P1A peptide pools, or a vehicle control (DMSO). The percentage of $CD8^+$ and $CD4^+$ T cells in the blood after prime-boost vaccination producing IFN-γ, IL-2 and TNF-α was then determined by ICS and flow cytometry. (B) DBA/2 mice were vaccinated with different vaccination regimes (as indicated) and bled 3 days before and 14 days after the MVA vaccination. PBMCs were stimulated *ex vivo* with 4 µg/ml of P1A peptide pools, or a vehicle control (DMSO). The percentage of IFN-γ^+ $CD8^+$ T cells after prime (closed circles) and boost (closed squares) in response to stimulation with P1A peptides vaccination was then determined by ICS and flow cytometry. Data are shown as the mean ± SEM and each symbol represents an individual mouse.

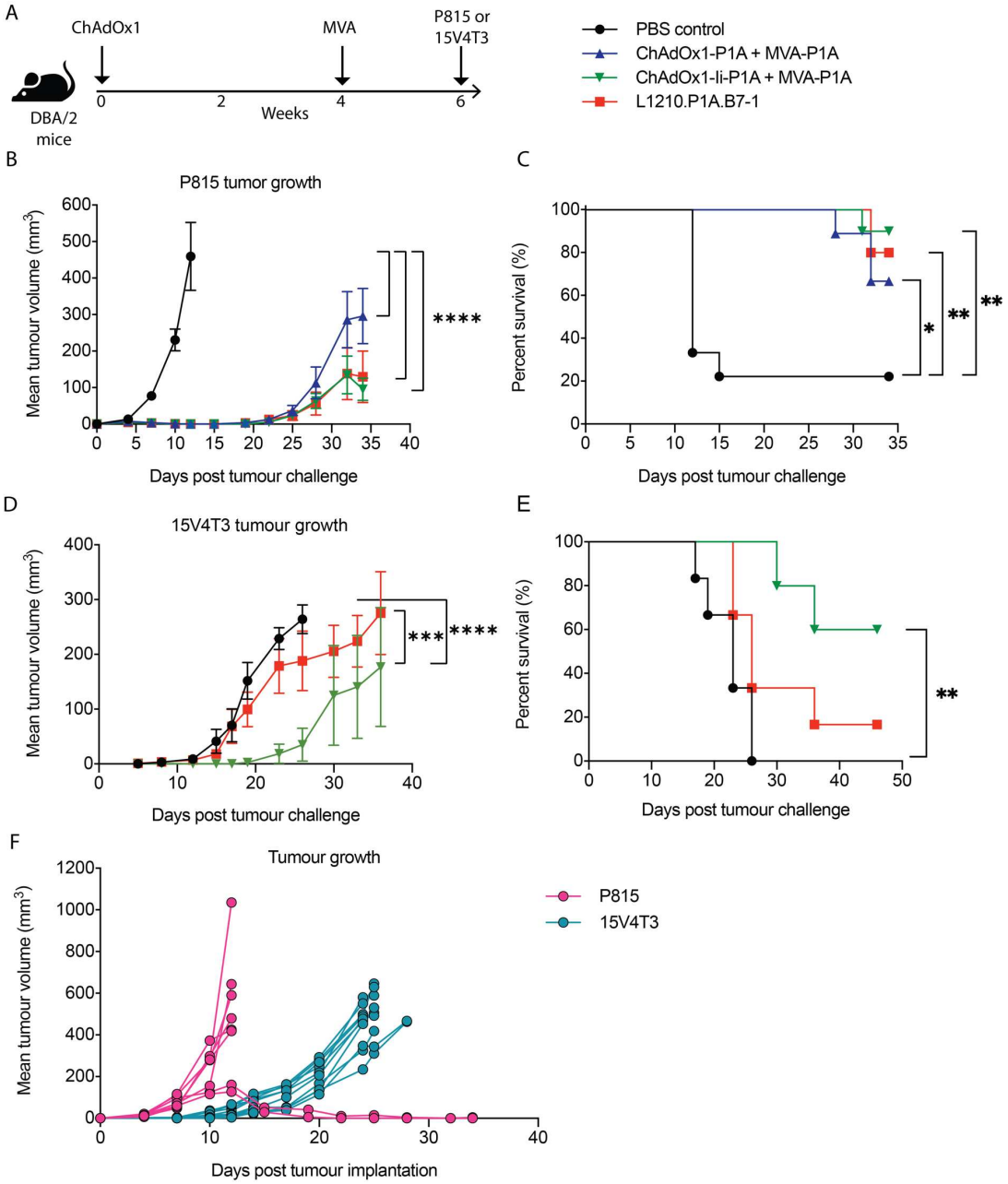

Figure S2: ChAdOx1/MVA P1A vaccination confers protection against P1A-expressing tumors. DBA/2 mice received a prime vaccination via intramuscular injection with 10^8 IU of ChAdOx1-P1A, ChAdOx1-Ii-P1A or a sham vaccination with PBS, then the ChAdOx1-P1A (± Ii) vaccinated mice received a boost vaccination with 10^7 PFU of MVA-P1A 4 weeks later. A fourth group received $1x10^6$ L1210.P1A.B7-1 cells via intraperitoneal injection. Two weeks after the MVA boost vaccination, all mice were implanted with either $1.5x10^6$ P815 or $1x10^6$ 15V4T3 cells in the right flank via subcutaneous (s.c.) injection. Tumor size was then measured and mice were sacrificed when tumor size reached 10 mm length in any direction. (A) Experimental timeline. (B-E) Mean tumor growth (B and D) and survival (C and E) for P815 and 15V4T3 challenged mice are shown. (F) Individual growth curves for P185 and 15V4T3 tumors from PBS control mice. Mean tumor growth data in B and D are presented as mean tumor volume (mm^3) ± SEM. Each group contained 5-10 mice, with data representative of 2 independent experiments. Statistically significant differences were determined by a two-way ANOVA followed by Tukey's post hoc test and statistical differences in survival data were determined by a log-rank test. *, $p \leq 0.05$, **, $p \leq 0.01$ ****, $p \leq 0.0001$.

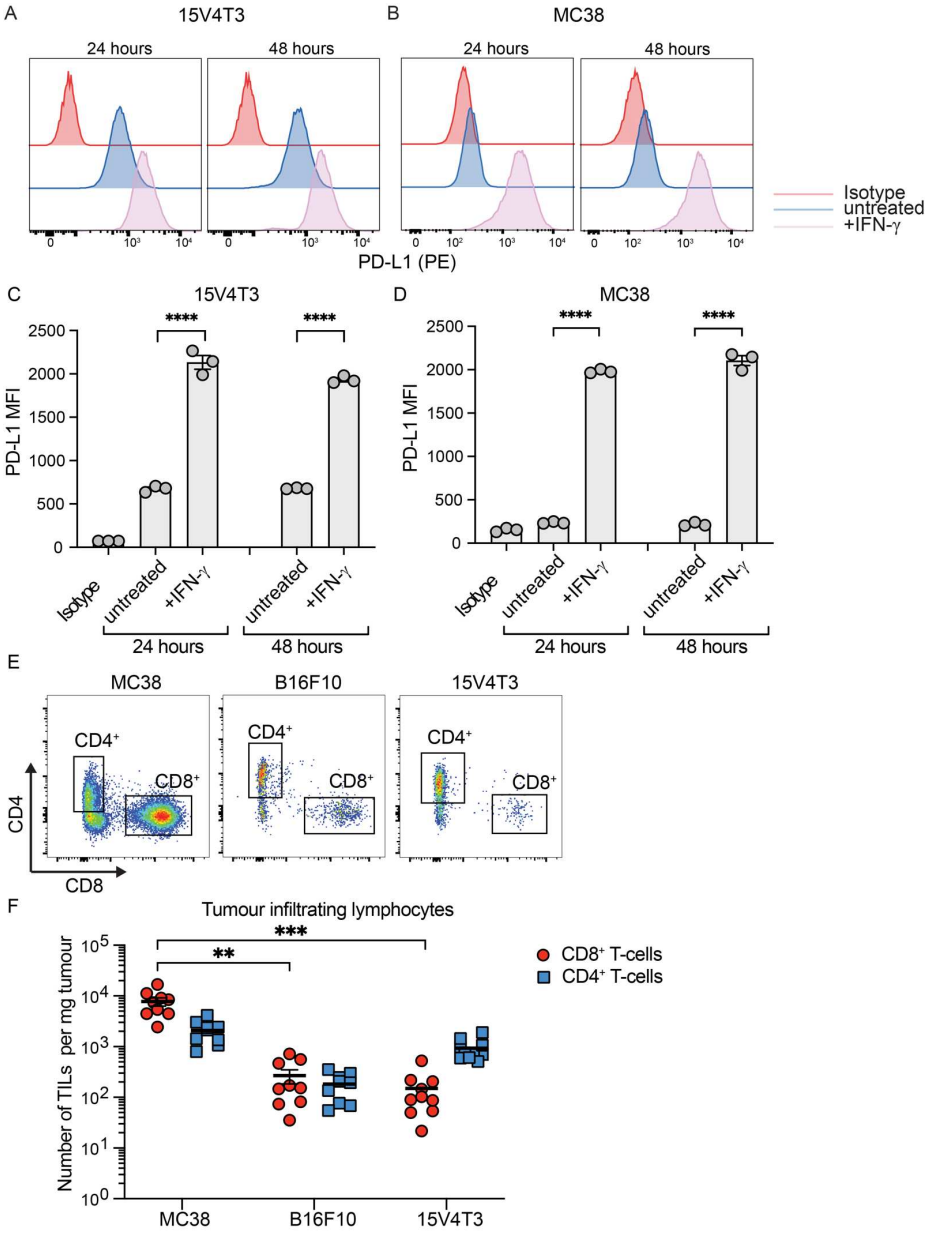

Figure S3: Surface PD-L1 expression level and CD8⁺ and CD4⁺ T-cell infiltration of murine tumor models. 15V4T3 and MC38 cells were cultured *in vitro* and stimulated with or without 20 ng/ml recombinant mouse IFN-γ for 24 or 48 hours. Cells were then stained with either PE-anti-PD-L1 or PE-IgG2b isotype control and the level of surface PD-L1 expression was assessed by flow cytometry. Representative flow cytometry histograms for PD-L1 expression level are shown for (A) 15V4T3 and (B) MC38. The PD-L1 mean fluorescence intensity (MFI) was calculated for (C) 15V4T3 and (D) MC38 cells. Each point shows an individual technical replicate (n=3 per group). Data are shown as mean ± SEM. Statistical differences between each group were calculated by ordinary one-way ANOVA followed by Tukey's post hoc test. ****, $p \leq 0.0001$**.** (E, F) BL/6 mice were implanted with either $1x10^5$ MC38 or B16F10 cells and DBA/2 mice with $1x10^6$ 15V4T3 cells via s.c. injection. Mice were sacrificed and tumors harvested when a size of 400-600 mm^3 was reached. Tumors were dissociated and the immune infiltrate was analyzed by flow cytometry. (E) Representative flow cytometry plots of CD4⁺ and CD8⁺ T cells, gated on live CD3⁺ cells from MC38, B16F10 and 15V4T3 tumors. (F) Total numbers of tumor infiltrating CD4⁺ and CD8⁺ T cells. Data are shown as mean ± SEM and each symbol represents an individual mouse, with n=9/10 mice per group. Statistically significant difference between groups was determined by a Kruskal-Wallis test with Dunn's multiple comparisons test. ** $p \leq 0.01$, ***, $p \leq 0.001$.

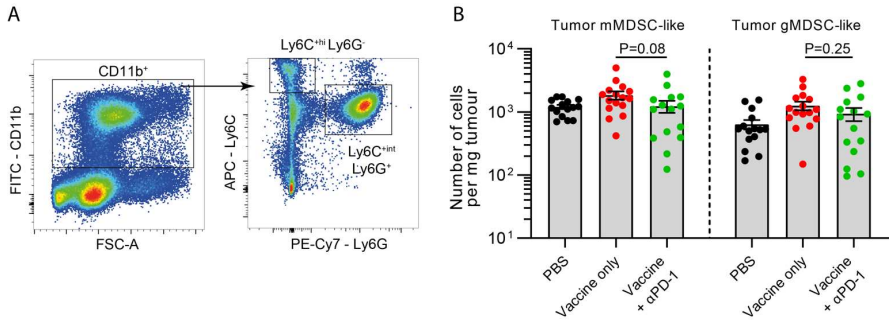

Figure S4: MDSC-like cell infiltration into 15V4T3 tumors. Mice bearing 15V4T3 tumors received ChAdOx/MVA P1A vaccination and were treated with anti-PD-1 as shown in Fig. 4A. Tumors were excised, processed to single cell suspension, and analyzed by flow cytometry. (A) Representative flow cytometry gating-strategy for mMDSC-like ($CD11b^+$ $Ly6C^{+hi}$ $Ly6G^-$) and gMDSC-like ($CD11b^+$ $Ly6C^{+int}$ $Ly6G^+$) cells. (B) Total numbers of tumor-infiltrating mMDSC-like and gMDSC-like cells as quantified by cytometry. Statistically significant differences between groups were compared by a Kruskal-Wallis test with Dunn's multiple comparisons test.

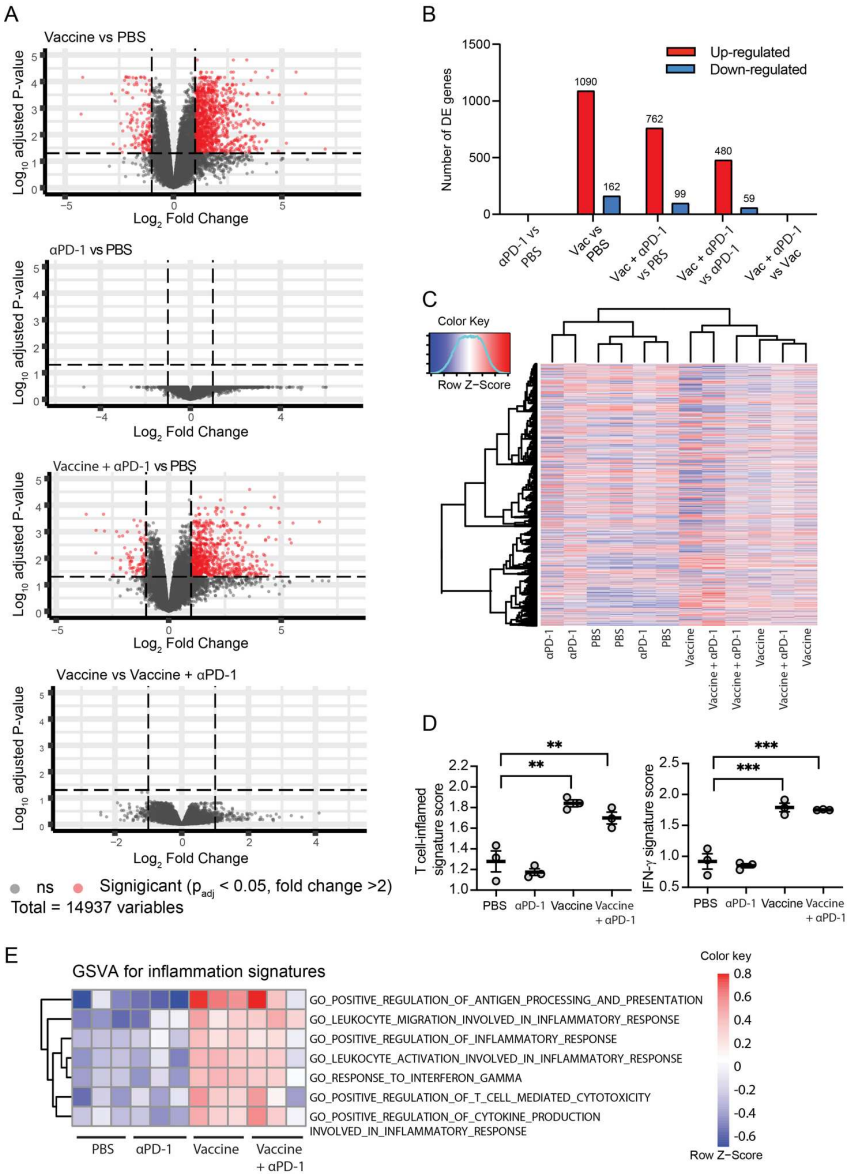

Figure S5: Bulk RNA-seq gene expression analysis of 15V4T3 tumors. 15V4T3 tumors were excised from the mice shown in Fig. 4 and RNA isolated from a small cutting of tumor tissue to analyze gene-expression at the transcriptional level. Tumor mRNA from each of 3 mice per group was sequenced on an Illumina NovaSeq 6000 as 150 bp paired-end reads. Following data processing, differential gene expression analysis between the anti-PD-1 only, vaccine only, and vaccine + anti-PD-1 combination treatment groups compared to the PBS control was performed using EdgeR software. (A) Volcano plots showing the distribution of differentially expressed genes (DEGs) between different experimental groups. Each point represents an individual gene, with significant DEGs shown in red. Dashed lines indicate the threshold set for significant differential expression of $\log_2FC > 1$ and $P_{adj} < 0.05$. (B) Number of DEGs identified in tumors in each of the experimental group comparisons (red upregulated, blue downregulated). (C) A heatmap showing log-CPM gene expression values of all expressed genes in the dataset for each sample. Expression across each gene (rows) has been scaled by calculation of a Z-score, indicated by the heatmap color key. Unsupervised hierarchical clustering was performed at both the gene (y-axis) and sample (x-axis) level and is shown in dendrogram format. (D) T cell-inflamed and IFN-γ gene expression signature scores for each sample. Data are shown as mean ± SEM. Statistically significant differences between group gene signature scores were determined by an ordinary one-way ANOVA with Tukey's post hoc test. **, $p \leq 0.01$, ***, $p \leq 0.001$. (E) GSVA was performed for each of the indicated gene sets and the results are visualized on a heatmap.

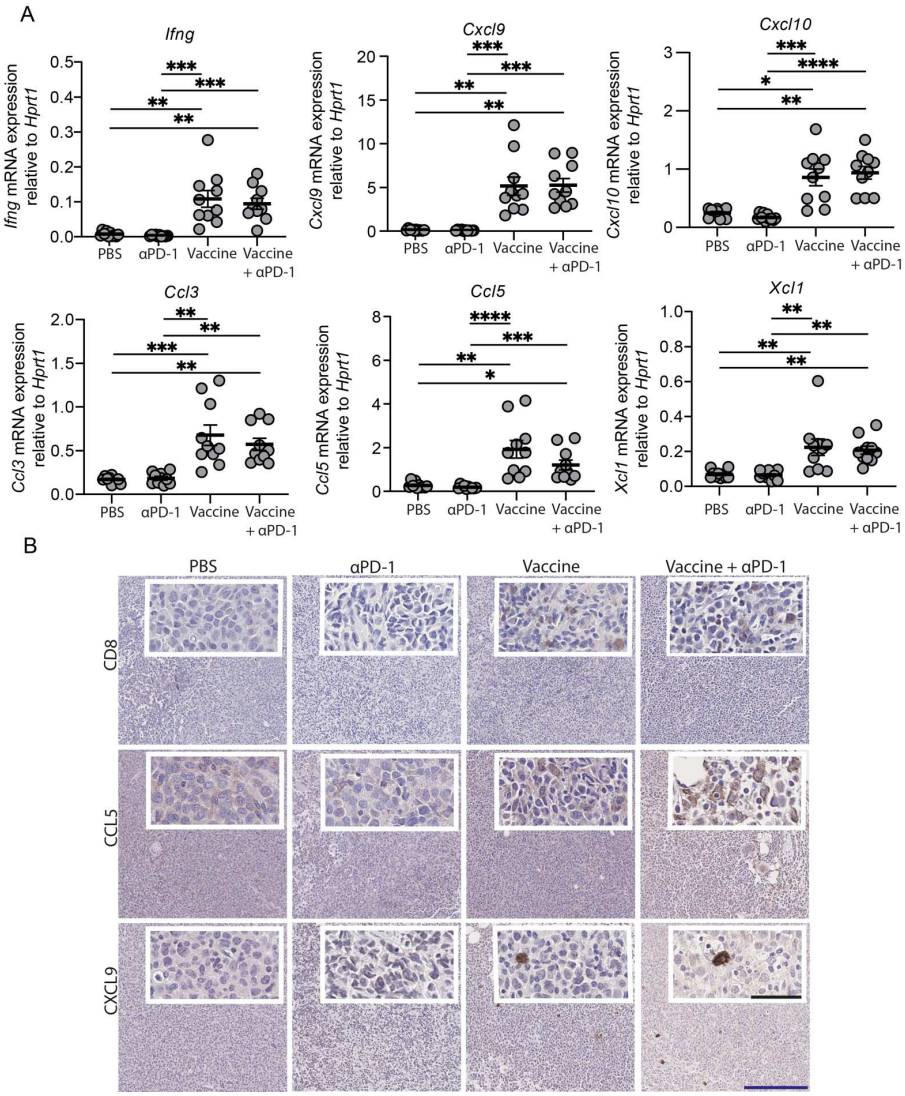

Figure S6: Assessment of pro-inflammatory mediator expression in the 15V4T3 tumor microenvironment. 15V4T3 tumors were excised from tumor-bearing mice vaccinated with ChAdOx1/MVA P1A and treated with anti-PD-1 as detailed in Fig. 4. (A) Tumor RNA was isolated to analyze gene expression of pro-inflammatory mediators. Expression of *Ifng*, *Cxcl9*, *Cxcl10*, *Ccl3*, *Ccl5*, and *Xcl1* mRNA in the tumor was quantified by RT-qPCR. Target gene mRNA expression level was normalized relative to Hprt1 and is shown as $2^{-\Delta Ct}$. Data are presented as mean ± SEM and each symbol represents an individual mouse, with n=10 mice per group. Statistically significant differences between groups were determined by a one- way ANOVA followed by Tukey's post hoc test. *, $p \leq 0.05$, **, $p \leq 0.01$, *** $p \leq 0.001$ ****, $p \leq 0.0001$. (B) A cross-section cutting of tumor tissue was formalin-fixed and paraffin embedded (FFPE). Tissue sections (4 µm) were prepared from FFPE samples and stained with antibodies against CD8, CCL5 and CXCL9. Representative images of staining are shown of tumors from PBS control mice and each of the indicated treatment groups. Scale bars: 50 µm (inset) and 250 µm (overview).

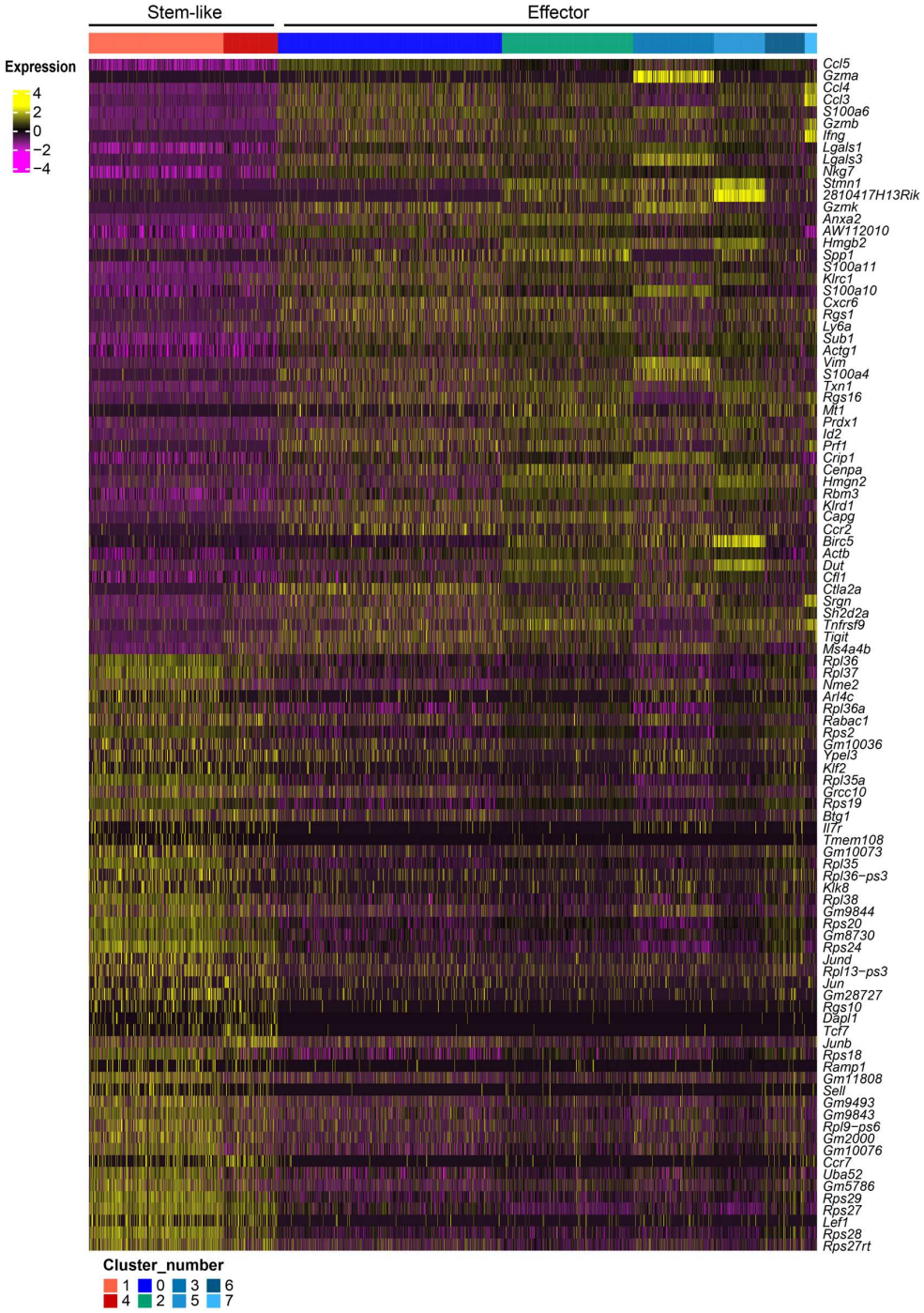

Figure S7: Heatmap of top 100 differentially expressed genes between stem-like and effector clusters identified by scRNA-seq of P1A$_{35-43}$-specific CD8$^+$ T-cells. 15V4T3 tumor-bearing DBA/2 mice were vaccinated with ChAdOx1-Ii-P1A/MVA P1A ± anti-PD-1 treatment (n=10 per group), tumors and spleens collected on day 25 and P1A$_{35-43}$-specific CD8$^+$ T cells isolated via H-2L^d P1A$_{35-43}$ tetramer staining and FACS as described in Fig. 5A. The transcriptional profile of P1A$_{35-43}$-specific CD8$^+$ T cells was determined via scRNA-seq using a 10X Genomics pipeline. Gene expression profiles of single cells separated into eight clusters by k-nearest neighbor clustering analysis using Seurat. The top 100 DEGs between the stem-like clusters and effector clusters are shown.

Table S2: P1A$_{35-43}$-specific CD8$^+$ T-cell gene signatures identified by scRNA-seq

SpleenCombi_vs_ spleenVac_UP			SpleenVac_vs_ spleenCombi_UP		TumorCombi_vs_ tumorVac_UP	TumorVac_vs_ tumorCombi_UP
Jund	Uba52	Gm2000	Gzmk	Vim	Areg	Vps37b
Taf10	Set	Ets1	S100a6	Emp3	Gm10709	Ifi27l2a
Chic2	Rps18	Nme1	Ccl4	Cdc42	H2-Q6	Rps8
Gnas	Arl2bp	Rps27rt	Ccl5	S100a4	Ccl4	Hsp90aa1
Alyref	Rpl9-ps6	Usf2	S100a10	Ywhaz	Gm8730	Cd7
Pcbp1	Emc10	Stk24	Klrc1	Arpc3	Gm9843	Slc3a2
Tprgl	Grb2	Rps2	Ms4a4b	Gimap7	Rps18	Rpl10
Ppp1cc	Rpl36-ps3	Gm10073	Nkg7	Actg1	Cox17	Pdcd1
Arf6	Hnrnpab	Gm5786	Ctla2a	Ifi27l2a	Uba52	Hsp90ab1
Rac1	E2f4	Capns1	S100a11	Tmem50a	Ccl3	Hspd1
Btg1	Srsf2	Rpl36a	Ier3	Cfl1	S100a4	Hnrnpa3
Pitpna	mt-Nd4	Ccni	Cd48	Thy1	Hcst	Serpinb9
Dcun1d5	Glrx5	Rpl6l	Lgals1	Cyba	Rpl27-ps3	Serpinb6b
Ypel3	Ptms	Gm28727	Lsp1	Lck	Rpl6l	Actb
Ube2s	Gm9493	Nme2	Sh2d1a	Hmgb2	Rps28	Hnrnpa1
Tmem243	Mkrn1	Rps26-ps1	Klrd1	Arpc1b	H2-Q1	Stat3
Tgfb1	Ccr7	2300009A05Rik	Ly6a	Cd3e		Mdh1
Hnrnpl	Ubald2	Gm8730	Calm2	AW112010		Eif4a1
Gnai2	Grk6	Rps20	Crip1	Actb		Sult2b1
Bag1	Mpnd	Gm9844	Lgals3	Tmsb4x		Stk17b
Cdc34	Aars	Rps19	Tigit	Cd52		Ifngr1
Ctbp1	Gnb1	Rpsa	Arl6ip5	Rac2		Gnb2l1
Klf2	H2-Ke6	Rpl35	Cd82	B2m		
Ybx1	Lamp1	Rpl12	Anxa2	Hcst		
Gm10076	Pdcd4	Gm11808	Laptm5	Pfn1		
Rab2a	1110008F13Rik	Rps21	Prr13	Sh3bgrl3		
March2	Rps28	Gm8186	Tagln2			
2310036O22Rik	Srm	Rps27	Sub1			
Mtch1	Gm10709	Rpl39	Ctsd			
Snf8	Lef1	Rps24	Sp100			
Bri3	Tmem108	Gm10260	Prdx1			
Arl4c	Rps29	Rpl3	S100a13			
Abhd17a	Erdr1	Rps7	Clic1			
Chmp4b	Efhd2	Rpl38	Zyx			
H2afy	Rpl13-ps3	Rpl10a	Pycard			
Nsmce4a	Pcbd2		Gabarapl2			
Rap1b	Pnrc1		Myl6			

Table S3: Gene sets corresponding to CD8⁺ T-cell dysfunctional and progenitor gene signatures from other published studies

CD39-CD69-	MEL_EXHAUST_Tirosh	CD8_B_Feldman	Exhaust_1_Feldman	Exhaust_2_Feldman	Exhaust_3_Feldman	Mem_Eff_4_Feldman	Early.Act_5_Feldman	Mem_Eff_6_Feldman	LCMV_PROG.EX_Miller	B16_PROG.EX_Miller	Stem_like_Baharom	TOX_SIG (Scott)	CD39+CD69+	CD8_G_Feldman	LCMV_TERMN.EX_Miller	B16_TERMIN.EX_Miller
KLF2	FCRL3	CD38	SPC25	GEM	CCL3	LMNA	ELL2	PLAC8	ID3	CCR6	Ctla4	IGKC	ENTPD1	IL7R	1810011H11RIK	GZMD
AQP3	CD27	CCL3	CDCA5	LAYN	EPSTI1	NR4A3	PFKFB3	S1PR1	CCR7	TCF7	Dapl1	AVIL	CD69	GPR183	ACOXL	GZMG
CLIC3	PRKCH	STMN1	ESCO2	VCAM1	CD38	GPR183	DTHD1	SORL1	CD83	AFF3	Socs3	TOX	RRM2	LMNA	CD244	GZMF
LINC00861	B2M	MYO7A	CDC45	RDH10	FASLG	CDKN1A	SMAP2	SELL	BACE2	CXCR5	Tox	KLRB1C	TYMS	NR4A3	RASD2	GZME
CD8B	ITM2A	GOLIM4	ZWINT	FAM3C	IFI44L	CCR7	FKBP5	TCF7	ITGA7	DAPL1	Gpr183	MEGF11	CD8B	TCF7	FCER1G	DSC2
FAM65B	TIGIT	VCAM1	SHCBP1	KIR2DL4	GIMAP6	S1PR1	AIM1	CCR7	TNFSF11	ID3	Nr4a2	SCD1	KIAA0101	MGAT4A	OSGIN1	RASD2
FGFBP2	ID3	WARS	DLGAP5	TNFRSF18	TRAFD1	KDM6B	TMEM39A	IL7R	IL1R2	SLAMF6	Xcl1	RP23-284K1.6	CCL3	CD55	CCL6	CCL9
RASA3	GBP2	HAVCR2	RAD51	MTSS1	LGALS9	ELL2	NR4A3	MGAT4A	SOSTDC1	OTX1	Rgs16	PIF1	TUBA1B	AIM1	CD200R2	LTF
C10orf54	PDCD1	LGALS9	KIF18B	CADM1	CXCR6	TIPARP	PER1	FAM65B	DAPL1	CD22	Rpl12	TNFRSF8	MKI67	PER1	GM10389	CCR1
SAMD3	KLRK1	ID3	RRM2	ENTPD1	RAB37	SC5D	TSPYL2	LTB	BMP7	TNFRSF25	Cd28	TMEM163	UBE2C	FOSL2	CDK14	1810011H11RIK
CD27	HSPA1A	PRDX3	BIRC5	ETV1	CCR5	PLK3	TTN	FLT3LG	GCAT	VAT1L	Id3	NR2F6	HLA-DQA2	EGR1	GPR56	IGSF5
FAIM3	SRGN	MCM5	TK1	AFAP1L2	ZBP1	CD55	TMEM2	PXN	FAM160A1	2610019F03RIK	Pou2f2	SERPINB6B	CDK1	TSPYL2	AA467197	GZMC
S100A10	TNFRSF9	LSM2	HJURP	TNFRSF9	SAMD9L	NR4A1	IL6ST	A2M	IL7R	HECTD2	Junb	FGR	STMN1	YPEL5	CSF1	HTRA3
LYAR	TMBIM6	MTHFD1	UBE2C	NAB1	SIRPG	REL	NAB1	ATM	TNC	MAPK11	Eef1b2	LRRK1	IL5	CSRNP1	SLC16A10	LTB4R1
BIN1	TNFRSF1B	FASLG	CCNB2	PELI1	MX1	PBX4	IQGAP2	C20orf112	SERPINA9	ART3	Rplp0	SUV39H2	NDFIP2	REL	GZMA	CD200R2
CTD-3184A7.4	CADM1	SNAP47	CENPW	DFNB31	HAVCR2	TNF	SLC7A5	GPR183	SLC43A1	TNFSF14	Rps15a	ESM1	DUSP6	SKIL	SFPI1	LGI2
KANSL1-AS1	ACTB	IFI35	GINS2	CTLA4	ACP5	IL7R	IPCEF1	EPB41	ART3	TNFSF8	Rps24	CENPE	CSF2	PIK3R1	RAC3	KLHL30
UBXN11	CD8A	SKA2	RAD51AP1	HSPB1	DDX60	RGCC	DCTN6	ADD3	PGCP	S1PR1	Ly6e	CCR2	XCL1	FOXP1	P2RY6	MGAT3
ZFP36L2	RGS2	NDUFB3	DTL	FKBP4	PDCD1	FOSL2	DUSP4	GRAP2	2610019F03RIK	FAM84A	Rpl6	KLRC1	UBE2S	RGCC	HTRA3	SERPINB9B
PPP2R5C	FAIM3	FABP5	SPC24	NAMPTL	SH2D3C	SIK1	RANBP2	KLRG1	WNT3	PGCP	Tcf7	NT5DC2	TOP2A	PFKFB3	IL20RA	GLIS1
LITAF	EID1	IFI27L2	CDCA3	MYO7A	GPR174	CSRNP1	FAM177A1	GIMAP5	TUBA8	LIF	Zfp36l1	CD244	HIST1H4C	MYADM	E230016K23RIK	FCRL6
ZNF683	HSPB1	PTTG1	PKMYT1	CXCL13	RPS6KA1	GPR132	GABARAPL1	TC2N	CCR6	TREML2	Rpl10a	ASPM	AIF1	ZFP36L2	GPR97	PRPH
S1PR1	RNF19A	ENTPD1	MELK	GOLIM4	GBP5	GLUL	RGPD6	TXNIP	WNT1	SYNPO	Rps20	FAM20A	TUBB	USP36	CHN2	LRRN4

CD39-CD69-	MEL_EXHAUST_Tirosh	CD8_B_Feldman	Exhaust_1_Feldman	Exhaust_2_Feldman	Exhaust_3_Feldman	Mem_Eff_4_Feldman	Early.Act_5_Feldman	Mem_Eff_6_Feldman	LCMV_PROG.EX_Miller	B16_PROG.EX_Miller	Stem_like_Baharom	TOX_SIG (Scott)	CD39+CD69+	CD8_G_Feldman	LCMV_TERMN.EX_Miller	B16_TERMIN.EX_Miller
TCF7	IFI16	EPSTI1	ANLN	PHLDA1	GBP1	KIAA1683	CTLA4	GIMAP2	SHANK1	SOSTDC1	Nsg2	ZDHHC2	CLSPN	TC2N	5031414D18RIK	HAVCR2
GIMAP4	LYST	PDCD1	CDCA8	DNAJA4	PTPN6	RALGAPA1	CREM	TNFAIP8	OAF	WNT10A	Rpl36a	UBASH3B	IFI27	FAM177A1	VILL	CD244
MYC	PRF1	TRAFD1	KIAA0101	TGIF1	S100PBP	PRNP	ETS1	IL16	MAGED1	KCNMB1	Rps27a	SAPCD2	HMMR	BTG2	KLRA3	5830473C10RIK
S1PR4	STAT1	SIRPG	GGH	HAVCR2	IFI35	PRMT10	PNRC1		MORN4	CD40LG	Rgs1	SCD2	EGR1	TSC22D2	KLRA7	RASSF6
CD52	UBC	RGS3	AURKB	APLP2	OAS3	SORL1	ZFP36L2		SCMH1	DTX1	Actn1	KIF20B	KPNA2	FAM65B	RANBP17	GPR56
STK38	CD74	UBE2F	ASF1B	GPR56	SNAP47	FAM177A1	RGPD5		NSG2	DHRS3	Bcl2	CCR5	TPX2	STAT4	S1PR5	GZMB
NEAT1	IL2RG	SNRPD1	CDC20	BPGM	GIMAP4	CHMP1B	ZNF331		PAQR8	SELL	Tnfaip3	ACSL3	ZWINT	RGPD5	GM4956	1300014I06RIK
LGALS3	FYN	FIBP	NCAPG	SEC14L1	PARP9	ZC3H12A	CNOT6L		KIT	ST8SIA1	Cd69	WEE1	TK1	NEU1	TYROBP	FILIP1
GZMM	PTPN6	CLTA	DHFR	TNIP3	IFNG	TSC22D2	TGIF1		BC048355	TNFRSF13B	Rps9	HMMR	CD38	IFRD1	HEYL	CDKN2A
SORL1	HLA-DRB1	CXCL13	KIFC1	METRNL	SIT1	P2RY8	CXCL13		4930583H14RIK	CXXC5	Jun	SH2D5	UBE2T	PDE4B	TIFAB	GPR97
AL592183.1	HNRNPC	NMI	TYMS	HSPH1	PYCARD	NEU1	PDE4D		TWIST2	PLA2G4F	Rps8	MYO1E	NUSAP1	NR4A1	KLRA9	AA467197
R3HDM4	UBB	DNPH1	CKAP2L	KLRC2	RGS3	TCF7	RNF19A		SLC12A8	XCL1	Rpl29	CENPF	PCNA		AGPAT9	ADAM8
MIAT	CD8B	PCNA	CLSPN	PMAIP1	XAF1	ZNF683			HSD3B7	CD83	Rps10	HAVCR2	CENPF		KLRB1C	CDH17
ANXA4	HAVCR2	ACP5	MLF1IP	DUSP4	OAS2	MYADM			TCF7	CYR61	Fam46c	EOMES	H2AFX		ENTPD1	FCER1G
LEF1	IRF8	MRPL28	TROAP	IGFLR1	C5orf56	ATP2B1			1700019D03RIK	KLF3	Rps28	PAK6	CRTAM		INSC	EPDR1
TSC22D3	LAG3	FARSA	KIF2C	HSPA1A	GIMAP5	CREM			H2-OB	S1PR5	Rpl21	AHR	ASPM		RAB3IL1	CHL1
IL7R	ATP5B	COX5A	WDR34	ZFAND2A	ABI3	OAT			ROPN1L	FAM160A1	Rpl7a	ARSB	GTSE1		CHIT1	IL1R2
P2RY8	STAT3	MRPL51	CDK1	NDFIP2	SNX20	NFE2L2			XCL1	SH2B3	Sidt1	KLRK1	TNFRSF18		GLP1R	CCL3
PLEC	IGFLR1	SNRPE	KIF23	PAM	VAMP5	DNAJB9			CD22	TESPA1	Traf1	IL10	MYBL2		HDHD3	SPP1
ERN1	MGEA5	RANBP1	PLK1	TP53INP1	IRF2	SKIL			FCRL1	LRIG1	Ppp1r15a	CKAP5	CKS1B		ATG9B	ACOXL
TSPAN32	HSPA1B	NOP10	TOP2A	AHI1	UBASH3A	DENND4A			TNP2	IL18	Crtam	ALYREF	SPC25		ARAP3	ENTPD1
S100A4	COTL1	PYCARD	NUF2	UBE2F	PARP10	SERTAD1			MMP10	NSG2	Rps18	GEN1	CDKN3		TRPC1	CALCA
SELL	VCAM1	GTF3C6	HMGB3	HSPA4	GIMAP7	YPEL5			FAM190A	SSPO	Rpl18a	IL24	IFNG		FAM19A3	CTNND2
RASGRP2	HLA-DMA	CCR5	ASPM	ICOS	GBP4	BCL6			LTA	TBC1D4	Dusp1	ECT2	AURKA		SERPINB1A	NEB
GADD45B	PDE7B	GSTO1	MCM2	CHORDC1	PVRIG	EGR1			DYNC2LI1	SH3BP5	Uba52	MKI67	FEN1		QSER1	LY6G5B

CD39-CD69-	MEL_EXHAUST_Tirosh	CD8_B_Feldman	Exhaust_1_Feldman	Exhaust_2_Feldman	Exhaust_3_Feldman	Mem_Eff_4_Feldman	Early.Act_5_Feldman	Mem_Eff_6_Feldman	LCMV_PROG.EX_Miller	B16_PROG.EX_Miller	Stem_like_Baharom	TOX_SIG (Scott)	CD39+CD69+	CD8_G_Feldman	LCMV_TERMN.EX_Miller	B16_TERMIN.EX_Miller
C11orf21	TBC1D4	OAS3	ORC6	TRPS1	CYTH4	PDE4B			DPYSL5	P2RX7	Rplp1	GTF2IRD1	GINS2		WDR31	UPP1
PIK3IP1	SNAP47	IGFLR1	CASC5	TBC1D4	DTX3L	ANXA1			AICDA	TNP2	Cd27	GZMA	CD40LG		RIPPLY3	AOAH
RNASET2	RGS4	HLA-DMA	CENPH	RALA	RHOC	SOD2			MNDA	SAMD3	Rpl15	HMGCS1	AURKB		PPP1R3B	MT2
S100A6	CBLB	STRA13	FEN1	CD82	SASH3	RNF125			TNFRSF26	FAM178B	Gnb2l1	BSPRY	NCAPG		STYK1	MREG
CCDC109B	TOX	HSD17B10	BRCA1	SEMA4A	CCL4L2	GADD45B			NME4	ZFP467	Cxcr3	ZBTB32	TNFSF10		CCL4	P2RY14
RAMP1	CALM2	VAMP5	MCM4	PON2	IFI6	SELK			DMRTA1	FAM81A	Rps4x	TUBB6	PLK1		FASL	ADORA3
RP11-640M9.1	ATHL1	NDUFAB1	TIMELESS	ACP5	BCAS4	RORA			STOM	SLC2A6	Rpl23a	BUB1	IL2RA		CDH17	EPAS1
GPR155	SPDYE5	BATF	MKI67	CCDC64	IKZF3	SELL			TMOD2	GALNT14	Rpl27a	ANLN	AGPAT9		ATP8A2	PLXND1
TXNIP	DDX5	NDUFS2	CDKN3	BHLHE40	GIMAP2	MXD1			SLFN5	GUCY1A3	Rpl34	SGOL2A	CCND2		ATF3	CDKN1A
CDC25B	SLA	C17orf49	APOBEC3B	NAMPT	ADORA2A	IFRD1			SLC22A17	PRSS2	Lag3	ULBP1	CENPE		4930515G01RIK	NPNT
ISG20	PTPRCAP	GNG5	CCNB1	AHSA1	ARPC5L	PIK3R1			LIF	AQP3	Rplp2	LMNB1	CDC20		H2-DMB1	3300005D01RIK
TRADD	IRF9	PSMB2	TPX2	BANP	GYG1	TUBB4B			GM17384	GZMM	Rpl39	CCNA2	CCNB1		LRRN4	FGL2
CRBN	MATR3	PDIA6	NCAPG2	RHBDD2	SLFN5	HECA			PTER	F2RL1	Eef1a1	COBLL1	SMC2		GZMB	ASB2
GIMAP7	LITAF	COMMD3	KIF11	CREM	CHST12	MPZL3			GM4814	OAF	Rpl14	HRAS	BIRC5		SEPN1	PPP1R3B
C16orf54	TPI1	CD63	TCF19	SLC7A5	APOBEC3D	USP36			SLAMF6	COLQ	Rps3	STK39	TUBA1C		SEPT4	IL10
FBXL8	ETV1	PSMA4	UBE2T	CACYBP	WARS	INSIG1			CLDN10	CCR7	Rpl28	FANCB	CCNA2		KCNJ8	GPR35
ODF2L	PAM	SAE1	SPAG5	NUSAP1	UBE2L6	LTB			JAM3	TNFSF11	Naca	SRSF2	CKS2		MRGPRE	ADRB1
LDLRAP1	ARID4B	ATP5J	BRCA2	STIP1	TMEM140	NR4A2			AFF3	TNFRSF26	PISD	MPP6	BIRC3		2900026A02RIK	MT1
MXI1	NAB1	MEA1	CCNA2	LRMP	CSK	SLC2A3			KIFC3	SLC15A1	Rpl17	FHL2	KRT7		PWWP2B	LAT2
RCBTB2	RAPGEF6	EXOSC9	BUB1B	PDE3B	F2R	PER1			CCDC116	BACH2	Rps19	KIF11	CENPW		ACTN2	D430041D05RIK
HSD17B11	LDHA	ARPC5L	CHEK1	RGS2	CTSS	S100A10			TNS1	EMB	Inpp4b	NCAPG2	MCM7		ETV5	RGS8
CLEC2B	WARS	BLOC1S1	BUB1	CCDC141	SLAMF7	AIM1			VIPR2	CXCR3	Zbtb32	FKBP5	ADAM19		CXCR6	OIT3
EMP3	RASSF5	HELLS	FANCI	SNAP47	CXCR3	MGAT4A			BCL2L14	NAPB	Rpl13	ANKLE1	TNF		TSGA10	RASL12
SH3BP5	OSBPL3	CXCR6	CENPM	DEDD2	CD27	CDC42EP3			GPR15	IL1RL1	Rps21	STIL	C15orf48		FGL2	SLC13A3
RP11-539L10.2	FAM3C	BCAS4	RNASEH2A	BTG3	PPP1R18	NDEL1			MAPK11	HEMGN	Limd2	PRC1	DLGAP5		PPP2R2C	SLC16A10

CD39-CD69-	MEL_EXHAUST_Tirosh	CD8_B_Feldman	Exhaust_1_Feldman	Exhaust_2_Feldman	Exhaust_3_Feldman	Mem_Eff_4_Feldman	Early.Act_5_Feldman	Mem_Eff_6_Feldman	LCMV_PROG.EX_Miller	B16_PROG.EX_Miller	Stem_like_Baharom	TOX_SIG (Scott)	CD39+CD69+	CD8_G_Feldman	LCMV_TERMN.EX_Miller	B16_TERMIN.EX_Miller
MIR142	TAP1	ETFB	HIRIP3	ITPRIP	TOX	IDI1			ENO2	ARC	Rpl37a	GPR141	DUSP5		EDARADD	PRF1
CLUAP1	HLA-DRB6	TXN2	MAD2L1	HSPA1B	CTSC	EIF4A3			9230110C19RIK	ANGPTL2	Rpl23	MTMR1	KIF11		FGD2	2810025M15RIK
YPEL3	FABP5	PTPN6	CCNF	GALNT2	SLAMF6	BIRC3			CXCR5	PRNP	Rps2	NFIL3	CCNB2		FCGR3	MYO10
SLCO3A1	CD200	SIT1	STMN1	TNFSF9	STAT1	TSPYL2			AFAP1	CD81	Rpl22	BUB1B	ACOT7		SYTL2	CD14
NOSIP	CTLA4	FKBP1A	SMC2	RANGAP1	FUT8	DCTN6			C3AR1	CRTAM	Rpsa	ITGAV	CASC5		IL10	CDKN2B
IL10RA	SNX9	COPZ1	CKS1B	PDCD1	IDH2	HSPH1			PRUNE2	POU6F1	Rpl8	SWAP70	PBK		6230409E13RIK	TSGA10
CD55	ETNK1	HLA-DRA	PAICS	DDX3Y	PCED1B	CDK17			SH3BP5	PLD4	Ighm	USP1	CDCA3		HAVCR2	WNT10B
RP11-395B7.4	MALAT1	CDC123	NCAPH	ARID5B	BST2	DDX21			SFMBT2	DNASE1L3	Rpl11	ENTPD1	TESC		EPDR1	BCMO1
MED15	ZDHHC6	AP2S1	ATAD5	DUSP10	PSMB10	PPP1R15B			NT5E	JUB	Cd9	RAC1	DUT		RAPSN	F2RL2
ATM	ARL6IP5	FUT8	PRC1	ZBTB1	STAT2	ZNF331			OASL2	ZHX2	Rps15	SGOL1	CENPM		SH3TC1	VIPR2
KLHL24	DUSP2	BST2	RFC5	SAMSN1	RNASET2	BTG2			1700025K23RIK	RAB37	Rpl32	NCAPG	KIF23		LRRC27	SYNPO2
ZNF276	HLA-DQB1	ATP6V1E1	CENPF	IRF4	RBCK1	AMD1			CCDC122	KLF4	Rpl24	PGP	ATAD2		PLEKHF1	2900026A02RIK
ANXA1	HNRNPK	CD2BP2	CENPN	CD2BP2	SEL1L3	SLC7A5			GSPT2	THA1	Fam101b	SPAG5	SGOL2		THRB	PPP2R2C
PLP2	DGKH	HLA-DQA1	CDCA7	SYNGR2	C14orf159	POLR3E			TREML2	SLC1A2	Rpl22l1	SLC25A13	TPM4		CISH	OPTN
AHNAK	LRMP	ZCRB1	CHTF18	CDK6	HLA-DRA	JMJD6			ISPD	GATSL3	Rps16	EMILIN2	AGTRAP		CCL3	DAB2IP
DDI2	H3F3B	MX1	CENPE	MCTP2	GZMA	CHD1			SELL	CMAH	Rpl5	TRIM59	MAD2L1		LAT2	ULBP1
VNN2	IDH2	TNFRSF9	WDR76	RAB27A	CD63	TAF13			AIPL1	CAR2	Gimap6	CCNB1	NDC80		TMPRSS6	CCL4
VCL	TRAF5	SQRDL	FBXO5	HSPD1	DENND2D	VPS37B			CLEC12A	ARL4D	Ltb	MASTL	NUDT1		PRDM1	CLGN
EPB41	TBL1XR1	SERPINB1	CDCA7L	NFAT5	HLA-DQB1	GTF2B			KBTBD11	TRAT1	Pacsin1	ASB2	CDT1		CD7	CCR5
DND1	ANKRD10	PHPT1	RFC4	BATF	PRF1	PAF1			CXCL10	SESN3	Mif	SRSF9	CENPA		LYN	SV2C
MAPKAPK5-AS1	ALDOA	CALM3	POLD1	GZMB	CD84	BCAS2			LRRC49	BCL6	Rps23	CDC25C	RPL39L		XCR1	CD55
CDC42SE1	LSP1	TOX	LRR1	NEU1	TIGIT	RGPD6			LRIG1	SLFN5	Smc4	MAN2A1	SHCBP1		GP49A	OSGIN1
PXN	PTPN7	SNRPC	RACGAP1	SYT11	CCL4L1	TUBA4A			P2RX7	MTMR7	Myc	KNTC1	CDCA8		F2RL2	CD200R4
SYNJ2	NSUN2	MRPS34	SNRNP25	CXCR6	PLSCR1	RASA3			SLC2A6	TLR1	Rpl3	AURKA	CEP55		CTNND2	CHN2
SIGIRR	RNF149	NUTF2	KNTC1	CNIH1	LAG3	GPCPD1			RAMP3	FAM53B	Cst7	TOPBP1	BRCA1		LIM2	SPATS2

CD39-CD69-	MEL_EXHAUST_Tirosh	CD8_B_Feldman	Exhaust_1_Feldman	Exhaust_2_Feldman	Exhaust_3_Feldman	Mem_Eff_4_Feldman	Early.Act_5_Feldman	Mem_Eff_6_Feldman	LCMV_PROG.EX_Miller	B16_PROG.EX_Miller	Stem_like_Baharom	TOX_SIG (Scott)	CD39+CD69+	CD8_G_Feldman	LCMV_TERMN.EX_Miller	B16_TERMIN.EX_Miller
PDE6G	CD2	NDUFS6	NUDT1	FCRL3	DAXX	RASGEF1B			ST6GAL1	CCDC64	Ifi27l2a	CEP55	ORC6		CELA1	GIPC2
SLAMF6	SRSF1	PSMB3	ACOT7	CRTAM	PHF11	DNAJA1			ESPN		Rpl9	UGCG	CISH		ABI3	JAM2
TIMP1	GOLPH3	CHMP2A	CDK2	TTN	IGFLR1	FAM46C					Rpl37		MX1			
	HLA-A	SLC25A11	GMNN	TOX	ATP6V1E1	PTP4A1					Itpkb					
	LIMS1	SHFM1	TMEM106C	MORF4L2	HLA-DQA1	TUBA1A					Rps3a1					
	SDF4	TMEM179B	LIG1	TIGIT	CMTM3	KPNA2					Rpl35					
	ROCK1	EIF6	FANCG	DCTN6	DNAJC4	ZFAND5					Ccr7					
	EDEM1	ANXA5	MXD3	MTHFD2	LASP1	SLC38A2					Eef1g					
	APLP2	JAKMIP1	PCNA	FUT8	HLA-DMA	PLIN2					Rps27					
	ITK	TALDO1	C19orf48	GATA3	NCKAP1L	HEXIM1					Odc1					
	TRIM22	GLRX3	POLA2	STAT5B	OASL	TMEM123					Rpl35a					
	SPRY2	ANAPC11	POLE	AKIRIN2	TMEM179B	JUND					Slamf6					
	ACTG1	DUT	NDC80	WHSC1L1	CCL4	MTRNR2L1					Rps26					
	HLA-DPA1	PDCD5	MCM3	STAT3	USB1	GABARAPL1					Rps11					
	EWSR1	ATP5G3	CDK4	ZEB2	UBE2F	STAT4					Rpl4					
	SRSF4	CHMP5	SLC43A3	MSI2	CHMP5	ALG13					Gimap7					
	ESYT1	TWF2	TUBG1	B3GNT2	C19orf66	FOSB					Emb					
	LUC7L3	IDH2	NME1	EIF4E	PPM1M	GPR65					Rpl36					
	ARNT	MPG	HAUS8	CKS2	ST8SIA4	SDCBP					Rps7					
	GNAS	SNRPF	MCM7	HSPE1	YARS	HBP1					Kbtbd11					
	ARF6	NDUFC1	NCAPD2	KPNA2	TBC1D10C	MAP3K8					Fosb					
	ARPC5L	GBP1	RFC2	NGRN	DRAP1	RANBP2					Rps5					
	NCOA3	DCTN3	SHMT1	PTPN11	POLD4	FAM129A					Rps29					
	PAPOLA	ERH	DTYMK	SNAP23	TRAPPC1	FOS					Rpl26					
	GFOD1	NDUFA12	PHF19	RASGEF1B	PKN1	DDIT3					Ipcef1					

CD39-CD69-	MEL_EXHAUST_Tirosh	CD8_B_Feldman	Exhaust_1_Feldman	Exhaust_2_Feldman	Exhaust_3_Feldman	Mem_Eff_4_Feldman	Early.Act_5_Feldman	Mem_Eff_6_Feldman	LCMV_PROG.EX_Miller	B16_PROG.EX_Miller	Stem_like_Baharom	TOX_SIG (Scott)	CD39+CD69+	CD8_G_Feldman	LCMV_TERMN.EX_Miller	B16_TERMIN.EX_Miller
	GPR174	LIMS1	POLD3	PFKFB3	JAKMIP1	CCNH					Rpl30					
	DDX3X	BANF1	DCTPP1	TNFRSF1B	LCP2	RGPD5					Rpl18					
	CAPRIN1	NDUFC2	POP7	CD27	CASP4	TUBA1C					Rps6					
	ARPC2	PSMC3	AHCY	TRIM13	APOL2	ATP1B3					Npm1					
	PDIA6	PON2	TEX30	ARNT	CASP1	GLIPR1					Psen2					
	SEMA4A	PRDX5	NUSAP1	SQSTM1	ABCA2	PRDM2										
	CSDE1	TMX1	DUT	MOB4	HLA-DRB5	EMD										
	PSMB9	STOML2	KIF18A	VPS37B	IFI27L2	HSPD1										
	NFATC1	RPS6KA1	MRPL17	ARL8B	SYNRG	MORF4L2										
		PAM	GGCT	TMEM140	ARHGAP30	IL21R										
		ATP5J2	CENPK	DNAJA1	IRF7	NFKBIA										
		GIMAP6	HAUS4	ZC3H7A	RARRES3	LYAR										
		NDUFB7	POLD2	GALM	HMOX2	DNAJB6										
		DBI	LMNB1	STAT5A	LSM2	TMBIM1										
		IFI6	BLM	CARD16	GZMH	PFKFB3										
		TSTA3	PRIM1	AMD1	ISG15	FAM65B										
		SSNA1	MT1E	RGCC	CHFR	MED29										
		ADORA2A	CDCA4	GOLGA4	TRPV2	B4GALT1										
		FDPS	RRM1	SDCBP	ZNHIT1	NXF1										
		CYC1	RBBP8	HNRNPLL	HLA-DPA1	BIRC2										
		PSMD4	NCAPD3	NR4A1	UBA7	ARHGAP26										
		FAM96A	TFDP1	BIRC3	ADAM8	SYAP1										
		OAS2	UNG	FBXW11	GOLIM4	DNTTIP2										
		ERCC1	ATAD2	TANK	SERPINB1	ETF1										
		PDHB	ACAT2	ASXL2	ATF6B	BTG1										

CD39-CD69-	MEL_EXHAUST_Tirosh	CD8_B_Feldman	Exhaust_1_Feldman	Exhaust_2_Feldman	Exhaust_3_Feldman	Mem_Eff_4_Feldman	Early.Act_5_Feldman	Mem_Eff_6_Feldman	LCMV_PROG.EX_Miller	B16_PROG.EX_Miller	Stem_like_Baharom	TOX_SIG (Scott)	CD39+CD69+	CD8_G_Feldman	LCMV_TERMN.EX_Miller	B16_TERMIN.EX_Miller
		CD27	HADH	EIF5	SHISA5	PBXIP1										
		SNRPA	PAFAH1B3	FKBP1A	ITGB7	MKNK2										
		UBE2L3	YEATS4	GSPT1	TMBIM4	DEDD2										
		MDH1	RPA3	JMJD6	TRAF3IP3	AKIRIN1										
		SDHC	TIMM10	PRDM1	GPR171											
		PSMG2	MCM5	LAPTM4A	TRAF5											
		C11orf48	FANCD2	IL21R	ARHGEF3											
		PSMA2	RAD51C	ARPP19	PSMB8											
		C7orf73	ICMT	FABP5	IL2RB											
		MRPS16	HIST1H1D	SAR1B	APOBEC3G											
		MCM7	LSM5	LYST	CALCOCO2											
		SNX20	SSRP1	EZH2	MPHOSPH9											
		AK2	HIST1H4C	HERPUD1	DTHD1											
		RBBP7	DPYSL2	TRAF5	LY6E											
		TIGIT	TTF2	ANXA5	PPCS											
		TMPO	EEF1E1	ZNF331	CAPN1											
		CTSB	NUP37	UBE2B	GBP2											
		PARP1	EBNA1BP2	HBP1	PYHIN1											
		USB1	CCDC167	SYTL3	FKBP1A											
		MRPS7	MSH2	GTF3C1	NUDT22											
		NHP2	FH	FAS	CTSD											
		ATP5I	DDX11	SPPL2A	TRIM14											
		PSMC1	MRPL12	ATXN1	SLC25A45											
		VDAC1	PRDX4	GGA2	KLRD1											
		CARD16	DNAJC9	C5orf15	UCP2											

CD39-CD69-	MEL_EXHAUST_Tirosh	CD8_B_Feldman	Exhaust_1_Feldman	Exhaust_2_Feldman	Exhaust_3_Feldman	Mem_Eff_4_Feldman	Early.Act_5_Feldman	Mem_Eff_6_Feldman	LCMV_PROG.EX_Miller	B16_PROG.EX_Miller	Stem_like_Baharom	TOX_SIG (Scott)	CD39+CD69+	CD8_G_Feldman	LCMV_TERMN.EX_Miller	B16_TERMIN.EX_Miller
		RNF181	ANAPC15	TSPYL2	UNC13D											
		PGAM1	ITGB3BP	PMF1	PSMB9											
		NT5C	MAGOHB	RBPJ	GSDMD											
		IRF2	MMS22L	POLR3E	IRF9											
		NUDT22	ACTL6A	RAPGEF1	MPG											
		NDUFA9	BOLA3	NOP58	MYO1F											
		SRI	USP1	EED	SLFN12L											
		GBP4	NABP2	CHST12	FERMT3											
		NDUFS8	MCM6	GTF2B	MUS81											
		PSMC2	RUVBL2	TMX4	APOL6											
		FPGS	VRK1	CCND2	C17orf62											
		PLSCR1	NCAPH2	PAPOLA	FCRL3											
		POLR2G	HELLS	FAM53B	ICAM3											
		COX8A	KIF22	CCT4	SP140											
		SLX1B	WHSC1	TRIM59												
		TRAPPC1	MYL6B	FXR1												
		ABI3	PDCD5	PPIL4												
		CBX5	SHMT2	LAG3												
		PSMD14	HIST1H1C	DNAJB6												
		UBE2L6	RANBP1	SMAP2												
		IFNG	SCCPDH	RP11-345J4.5												
		DECR1	HAUS1	GPBP1												
		ITGB1BP1	MRPS23	SERTAD1												
		AKR1B1	UBR7	PAG1												
		PSMA5	POLR2H	TRIM26												
				TCP1												
				AZIN1												